ANL-ART-211
ANL-METL-25

Thermal Hydraulic Experimental Test Article – Status Report FY2020

Nuclear Sciences and Engineering Division

ANL-ART-211
ANL-METL-25

Thermal Hydraulic Experimental Test Article – Status Report FY2020

M. Weathered, D. Kultgen, E. Kent, C. Grandy, T. Sumner, A. Moisseytsev, T. Kim

Nuclear Sciences and Engineering Division
Argonne National Laboratory

October 2020

TABLE OF CONTENTS

LIST OF FIGURES

LIST OF TABLES

1. Executive Summary

The Thermal Hydraulic Experimental Test Article (THETA) is a facility that will be used to develop sodium components and instrumentation as well as acquire experimental data for validation of reactor thermal hydraulic and safety analysis codes. The facility will simulate nominal conditions as well as protected/unprotected loss of flow accidents in a sodium-cooled fast reactor (SFR). High fidelity distributed temperature profiles of the developed flow field will be acquired with Rayleigh backscatter based optical fiber temperature sensors. The facility is being designed in partnership with systems code experts to tailor the experiment to ensure the most relevant and highest quality data for code validation.

THETA is comprised of a traditional primary and secondary system. The primary system is submerged in the pool of sodium and consists of a pump, electrically heated core, intermediate heat exchanger, and connected piping and thermal barriers (redan). The secondary system, located outside of the sodium pool, consists of a pump, sodium to air heat exchanger, and connected piping and valves.

Figure 1 illustrates the main components of the primary system. THETA will be installed in the Mechanisms Engineering Test Loop (METL) with the primary system in the 28 inch Test Vessel #4, Figure 2. The design work for the facility has been completed. Since the FY19 THETA status report, [1], the THETA primary system components have been assembled and tested using de-ionized water. Some results of this testing at select Richardson and Reynolds numbers are included herein.

The custom THETA sodium flowmeter (permanent magnet submersible sodium flowmeter) has been built and calibrated using sodium in an auxiliary facility against a NIST traceable vortex shedder type flowmeter. The permanent magnet flowmeter showed excellent performance, following the theoretical equation for measured voltage quite well, with an error < 3.5% at flow rates ranging from 3-24 GPM at temperatures up to 400 °C.

The secondary sodium system for heat rejection from intermediate heat exchanger has been analyzed according to ASME code. All secondary side piping, fittings and a U-stamped air-to-sodium heat exchanger have been procured.

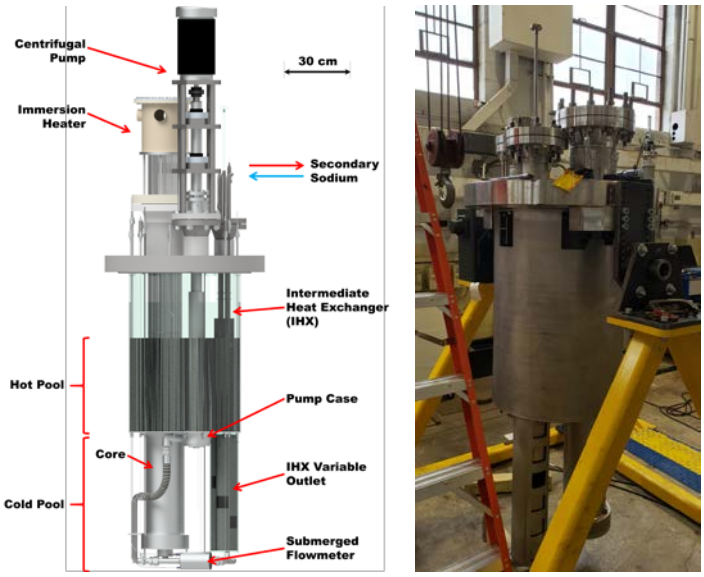

Figure 1: THETA Primary Heat Transport System (28 inch test vessel not shown)

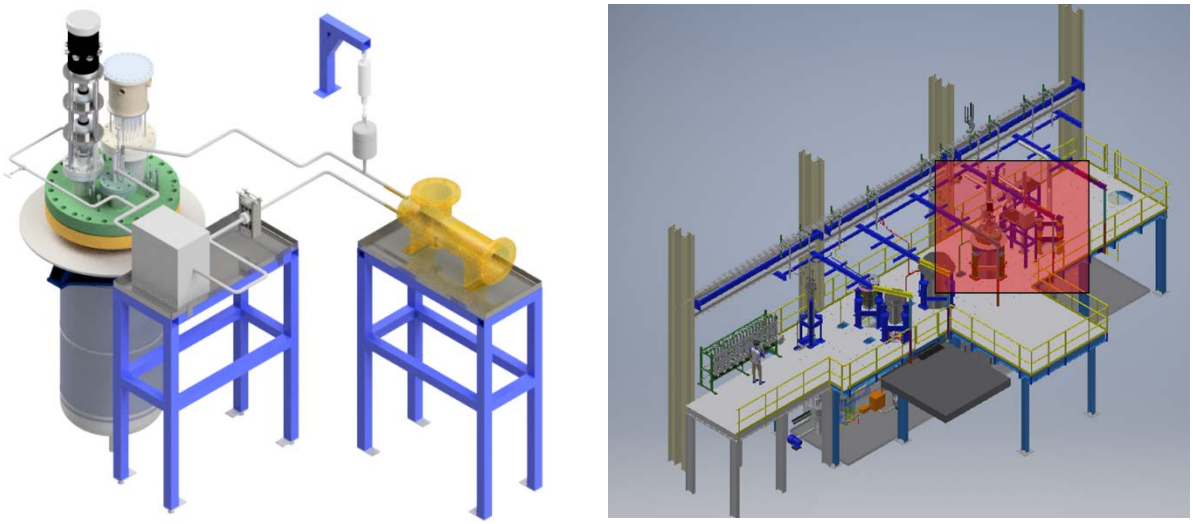

Figure 2: Isometric drawing of THETA primary vessel and secondary system left. Location of THETA in METL facility highlighted with red square, right.

2. Introduction

The Thermal Hydraulic Experimental Test Article (THETA) is a METL vessel experiment designed for testing and validating sodium fast reactor components and phenomena. THETA has been scaled using a non-dimensional Richardson number approach to represent temperature distributions during nominal and loss of flow conditions in a sodium fast reactor (SFR), this analysis was detailed in the THETA FY19 report [1]. The facility is being constructed with versatility in mind, allowing for the installation of various immersion heaters, heat pipes, and heat exchangers without significant facility modification. THETA is being designed in collaboration

with systems code experts to inform the geometry and sensor placement to acquire the highest value code validation data.

2.1. System Overview and Systems Code Application

THETA possesses all the major thermal hydraulic components of a pool type sodium cooled reactor. Figure 3 shows the piping and instrumentation diagram (P&ID) for the primary and secondary sodium circuit. A cross section of the primary vessel shows the pool and core geometry, Figure 4. As can be seen, a 28" METL test vessel is used for the primary sodium "reactor" vessel. An isometric model of the primary/secondary vessels, inter-vessel piping, and air-to-sodium heat exchanger (AHX) can be found in Figure 2.

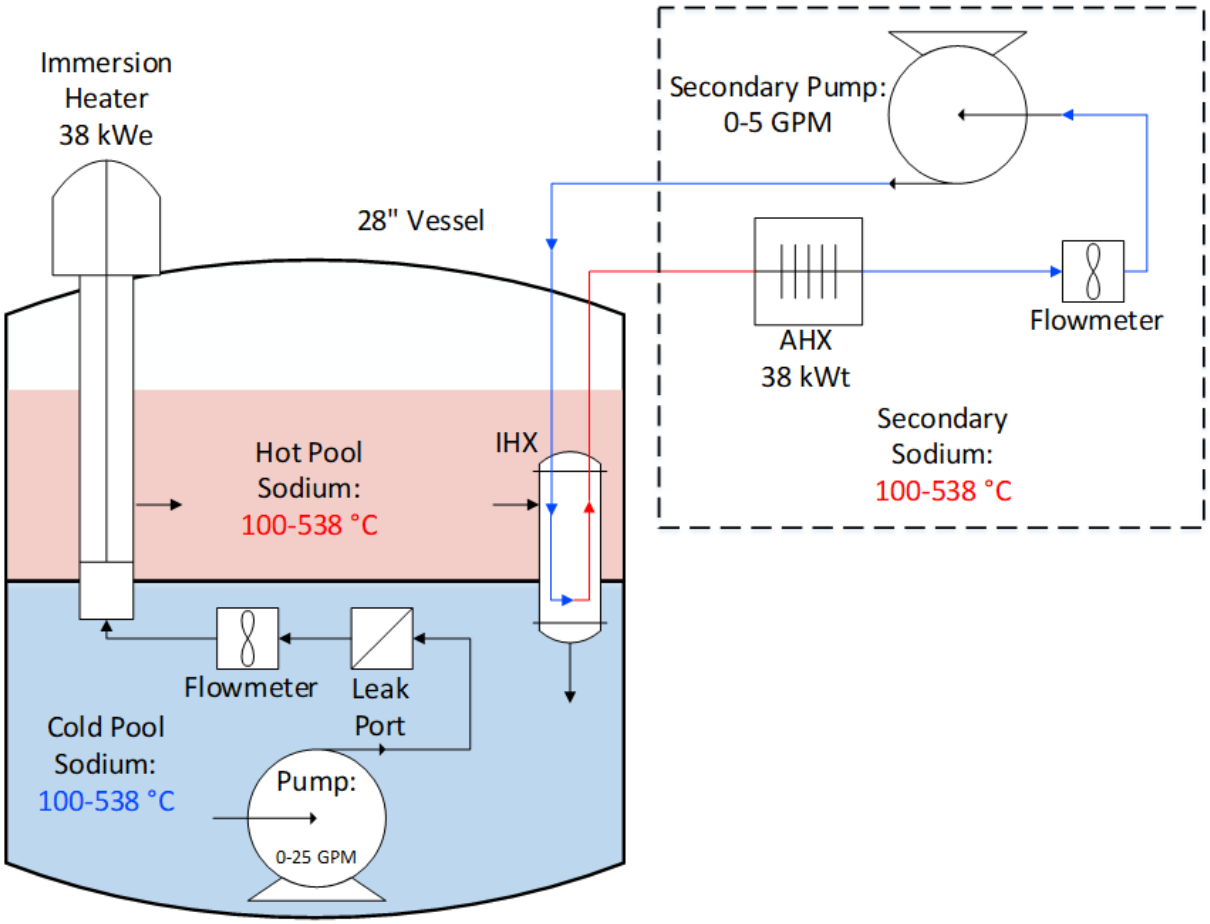

Figure 3: P&ID schematic of THETA

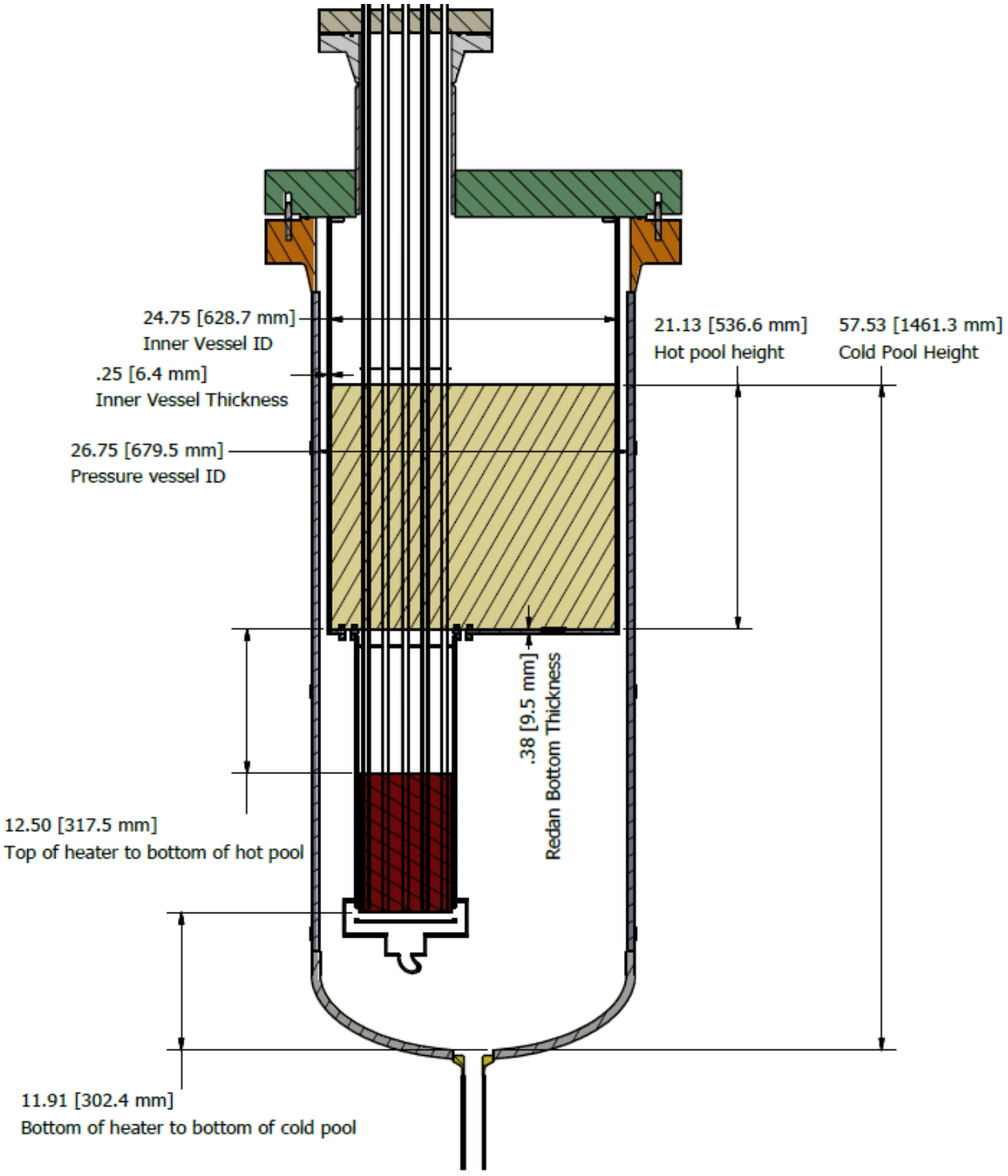

Figure 4: THETA pool and core geometry. Core nominal diameter: 0.2 [m] (8”), core heated length: 0.3 [m] (12”) see heater geometry in Figure 41 for more information

Argonne National Laboratory's SAS4A/SASSYS-1 computer code is used for thermal hydraulic and safety analysis of power and flow transients in liquid metal cooled reactors. Figure 5 gives a graphic displaying the segments and compressible volumes used to perform the deterministic analysis of anticipated events such as protected/un-protected loss of flow reactor trips etc. While SAS4A/SASSYS-1 was benchmarked against tests in historic reactors, such as EBR-II [2], a modern liquid metal thermal hydraulic facility is required for further system's code validation.

A parameter of interest is the differential in elevation between the intermediate heat exchanger (IHX) outlet and the core outlet. This differential will dictate the thermal stratification in the cold pool, thus driving the development of particular natural convection phenomena during reactor trips. The natural convection phenomena in the cold pool can then affect the thermal stratification in the reactor hot pool as sodium temperature from compressible volumes (CV) 3-5 (cold pool) will be transmitted to CV 1-2 (hot pool) in the SAS4A/SASSYS-1 computer code.

Please see [1] for an overview of the current systems code modeling efforts as applied to THETA.

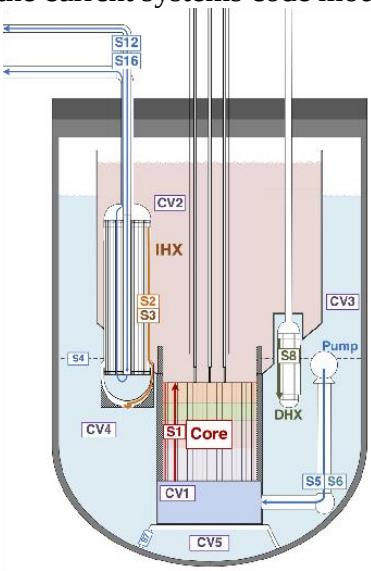

Figure 5: Schematic of SAS4A/SASSYS-1 showing locations of various compressible volumes (CV#) and segments (S#)

3. Primary Vessel Component Summary

The following section presents a summary of all primary vessel components as of September 2020, Figure 6. The primary and inner vessel was receieved early February 2020 and dry assembly and testing of all components dry and in deionized water has commenced.

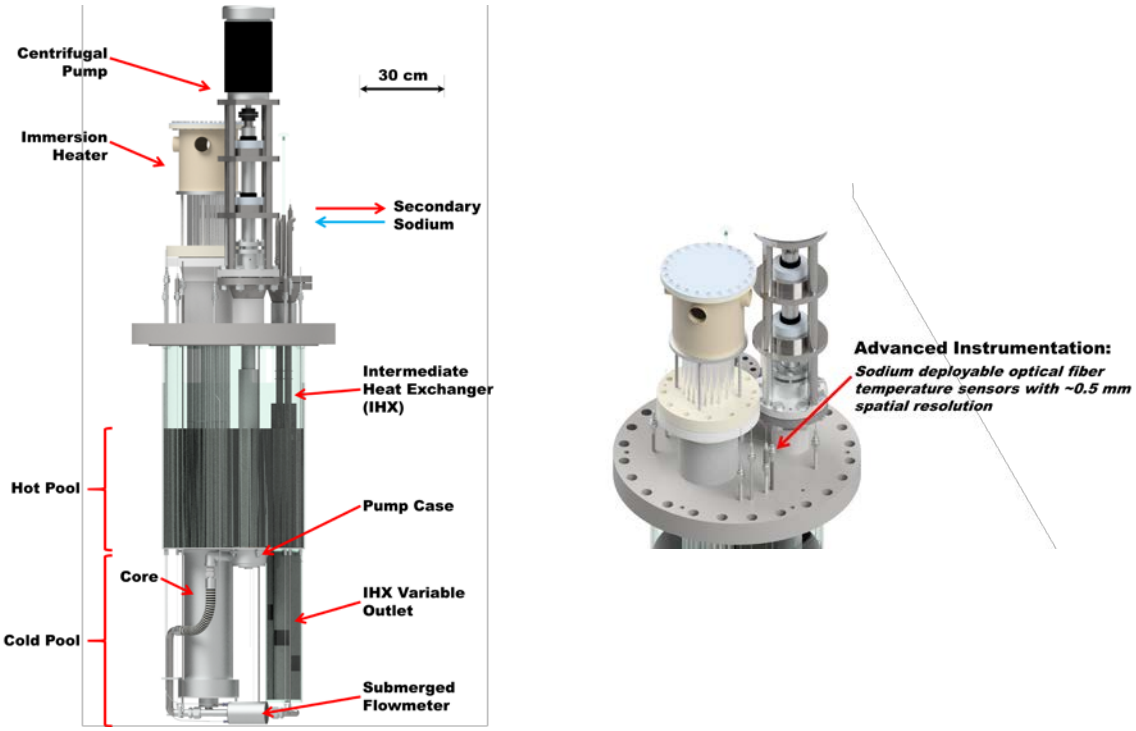

Figure 6: THETA primary vessel components

3.1. Primary Flange and Inner Vessel

The primary, 28" flange was received from the manufacturer in February 2020, Figure 7. A documentation package was also received which included a certificate of conformance to the original build specifications, a final inspection and packing checklist, all material test reports, the ASME data report, a test report from the hydrostatic pressure testing, liquid dye penetrant reports, radiography examination reports, and the dimensional inspection drawings.

The maximum allowable working pressure for the primary flange is 100 PSIG at 1200 °F. The minimum design temperature is -320 °F at 100 PSIG. A hydrostatic pressure test was performed on the primary flange at a test pressure of 427 PSIG. A helium leak test was also performed with the flange internals under vacuum with a leak rate ranging from 0.94-1.9 $x10^{-9}$ STD cc/sec.

Figure 7: 28”, 400# ANSI flange, THETA primary system

The primary flange was mounted to the METL test article flipper, a steel A-frame with 2 bearings that mount to a 28” METL test article Figure 8. This allows for fine adjustment of the angle of the flange to facilitate component and instrument installation.

Figure 8: A-frame test article ‘flipper’, left. Bearing with gear box used to rotate flange 360 degrees.

The primary flange can be seen mounted in the flipper and rotated 90 degrees to the horizontal, Figure 9. In this orientation the wetted face was then inspected to ensure surface finish of 32 µin Ra for mating with energized spring seal.

Figure 9: THETA primary flange mounted to flipper, positioned 90 degrees to the horizontal showing the wetted raised face

After mounting the primary pump and immersion heater onto the primary flange, sections 3.5 and 3.6, the inner vessel was then mounted to the primary flange, Figure 10. As can be seen the primary flange was rotated 'upside-down' to allow for careful installation of the inner vessel and to allow for small adjustments to ensure proper clearance for the primary pump shaft through the bottom of the inner vessel.

Figure 10: Initial installation of inner vessel on primary flange

After installation of the inner vessel, it was discovered that the three auxiliary flange heights and the cylindricity of the inner vessel side walls were outside of specification, causing interference issues between components and the penetrations in the bottom of the inner vessel, Figure 11.

Figure 11: Penetration of centrifugal pump shaft through bottom of inner vessel. As can be seen the initial lineup of the pump shaft to the vessel penetration was not centered.

In order to remediate these interference issues, the flange was transported to Argonne Central Shops where the flange was placed on a large CNC mill, Figure 12. The 'wetted' flange face was then oriented to be planar with the mill's X-Y plane, and it was confirmed that the flange face met the 0.005" flatness tolerance called out in the original design drawings, Figure 13. The mill z-axis could then be indicated off of the wetted face of the primary flange to determine the heights of the three auxiliary flanges.

Figure 12: Installation of primary flange on CNC mill machine

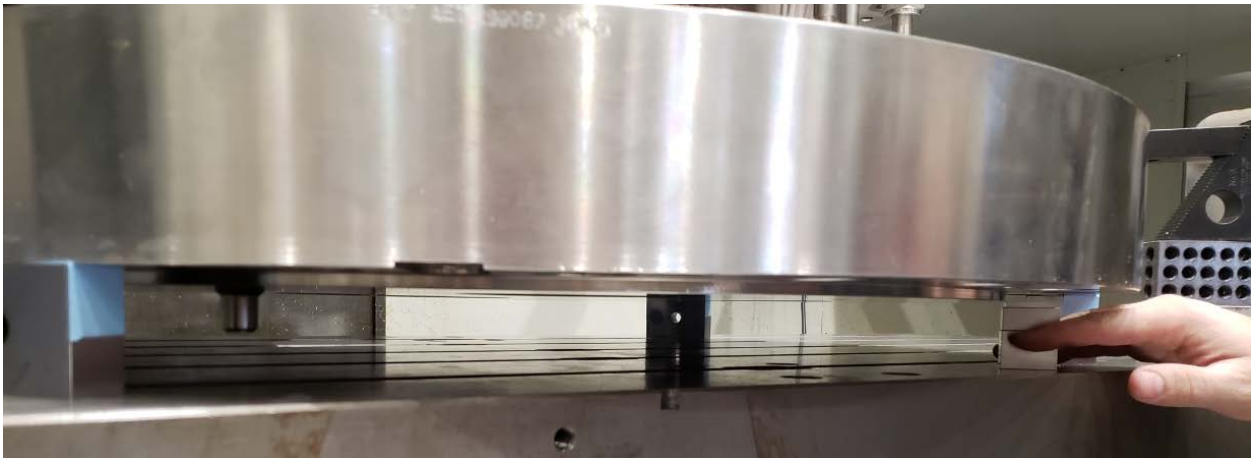

Figure 13: Confirming flatness of primary flange raised face to ensure parallelism with CNC mill x-y plane

The difference in elevation between the 28” flange face and the face of each of the auxiliary flanges were measured at four equidistant locations along the outside of the raised face, Figure 14 and Figure 15. Table 1 provides the nominal (as drawn) dimension, the as-built dimension and the differential from nominal. As can be seen, a tolerance of 0.01” was provided for the differential in elevation, the 8” flange was -0.044” out from nominal, the 5” flange was +0.104” out from nominal and the 4” flange was +0.076” out from nominal.

Figure 14: Dial indicating difference in elevation between raised face of primary 28" flange to each auxiliary flange raised faces

Figure 15: 8" Flange, left. 5" flange, middle. 4" flange, right.

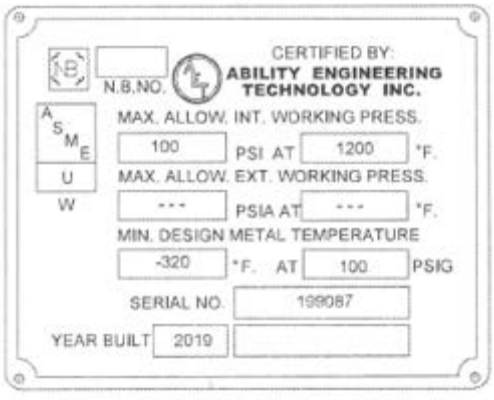

Figure 16: Primary flange nameplate

Table 1: Primary flange, auxiliary flange nominal dimensions (distance between raised faces), as built dimension and difference of nominal and as built.

Flange	Nominal Dimension	As Built	Out from Nominal
8”	15.88 ± 0.01	15.836	-0.044
		15.842	-0.038
		15.847	-0.033
		15.838	-0.042
5”	12.00 ± 0.01	12.104	+0.104
		12.070	+0.070
		12.049	+0.049
		12.080	+0.080
4”	11.14 ± 0.01	11.216	+0.076
		11.205	+0.065
		11.197	+0.057
		11.205	+0.065

Given the 4” and 5” 300# flanges, which mount to the intermediate heat exchanger and primary pump respectively, had face dimensions that were slightly greater than nominal, material could be removed from the raised face of the flange to bring the dimension within tolerance. The 8” flange face distance was closer to the wetted flange than specified in the drawings, therefore material could not be removed from the 8” 300# flange to bring within spec and this flange was not modified. The ASME certified manufacturer of the flange was contacted and asked to provide the minimum calculated thicknesses for the auxiliary flanges to ensure that the flange would still be stamped and rated to the maximum allowable working pressure of 100 PSIG at 1200 °F. The minimum calculated thicknesses for each flange are provided in Table 2.

Table 2: Calculated minimum thickness of each auxiliary flange to satisfy ASME BPVC

Flange	Minimum calculated Thickness to Satisfy Code	Final Thickness After Modification:
4”	0.8264”	1.21”
5”	0.8140”	1.27”
8”	1.0376”	Not Modified

The 4” and 5” flange faces thicknesses were reduced with the mill to bring within specification, Table 1, Table 2. After reducing the flange thicknesses, the energized spring seal grooves were re-machined to the correct specification and the raised face was re-established by removing material from the bolt circle.

A cylindricity of 0.005” was called out in the original design drawings for the inner vessel. A deviation from cylindricity of up to 0.080” was measured on the inner vessel upon inspection at Argonne Central Shops. In order to de-couple the cylindricity of the inner vessel side walls from

the penetration locations in the bottom plate of the vessel, a different inner vessel to primary flange mounting scheme was devised.

As can be seen in Figure 17, qty (3) 1.5” diameter 304 stainless shafts are used to support the inner vessel from the flange. The straightness of the 1.5” shafts may be constrained to a relatively higher tolerance to position the bottom plate of the inner vessel precisely, as compared to relying on the inner vessel side walls for positioning. The qty (3) shafts are attached to the primary flange via 5/8”-11, 316 stainless steel studs. In order to reduce the likelihood of galling occurring between the shafts, studs and flange, Nitronic-60 helicoil inserts were used on all of the threaded connections in this assembly. At the attachment point between the qty (3) shafts and the bottom plate of the inner vessel, 1.125” diameter holes were bored and 3/8” thick washer plates are sandwiched on either side to seal the gap between the 5/8” studs and the oversized holes.

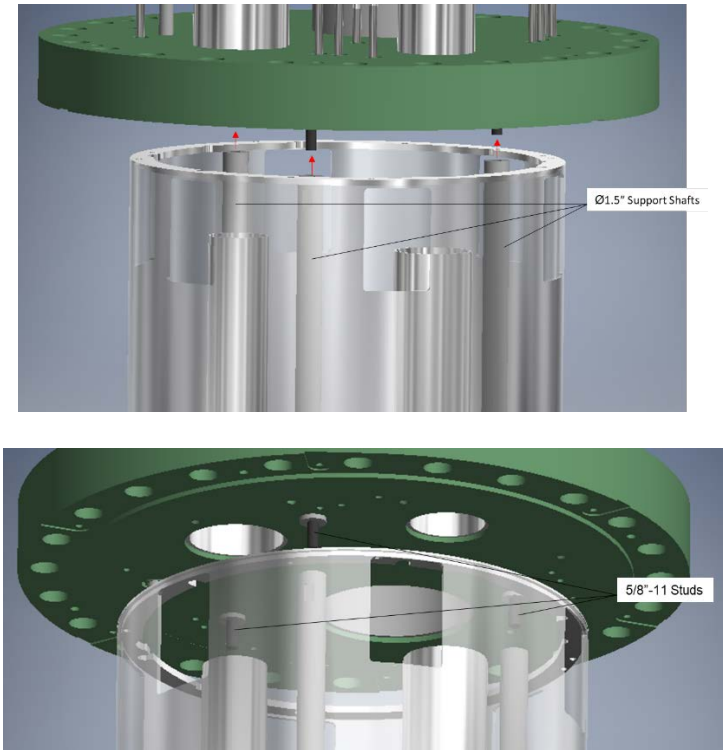

Figure 17: Drawing showing inner vessel offset from flange to illustrate support rod mounting location for inner vessel, top, mounting locations with studs installed in primary flange for support rods, bottom.

As can be seen in Figure 18, the primary flange was positioned on the CNC mill to drill and tap the 5/8-11” Helicoil threads for the support shafts. Figure 19 shows the inner vessel mounted to a CNC machine to drill the 3 mounting holes for the support shafts and to remove 1/16” of material off of the top ring of the inner vessel to elminiate contact between the inner vessel and the primary flange.

Figure 18: Primary flange positioned to bore 3X holes for 5/8" -11 STI tap for Nitronic-60 helicoil thread inserts to mount inner vessel support shafts

Figure 19: Inner vessel mounted to CNC machine for modifications

Figure 20 is a photo from inside the bottom of the inner vessel showing the three 1.5" diameter support shafts and Figure 21 is a photo of THETA dry assembly near completion.

Figure 20: Photo from inside the bottom of the inner vessel looking up towards the primary flange, the support shafts, intermediate heat exchanger shell and column pipe for the centrifugal pump are visible

Figure 21: Photo of THETA after dry assembly and prepared for water testing

3.2. Instrumentation

Table 3 summarizes THETA instrumentation which includes single and multi-point thermocouples, distributed optical fiber temperature sensors, and flowmeter voltage measurements. The port locations on the top flange have been labeled in Figure 22.

Table 3: THETA instrumentation and measurement. Port positions provided in Figure 22

Port #	Instrument	Measurement
1	Single TC	Heater inlet temperature
2	Single TC	Heater outlet temperature
3	Fiber	Hot and cold pool temperature
4	Rake TC	Hot and cold pool temperature
5	Rake TC	IHX outlet temperatures
6	Rake TC	Hot and cold pool temperature
7	Fiber	Hot and cold pool temperature
8	Rake TC	Outside inner vessel cold pool temperature
9	Rake TC	Hot and cold pool temperature
10	Fiber	Hot and cold pool temperature
11	MI Cable	Flowmeter voltage
12	Single TC	Flowmeter temperature
13	Fiber	Hot and cold pool temperature
14	Fiber	IHX temperature
15	Rake TC	IHX temperature
16-20	Single TCs	Heater temperatures, 3” above inlet

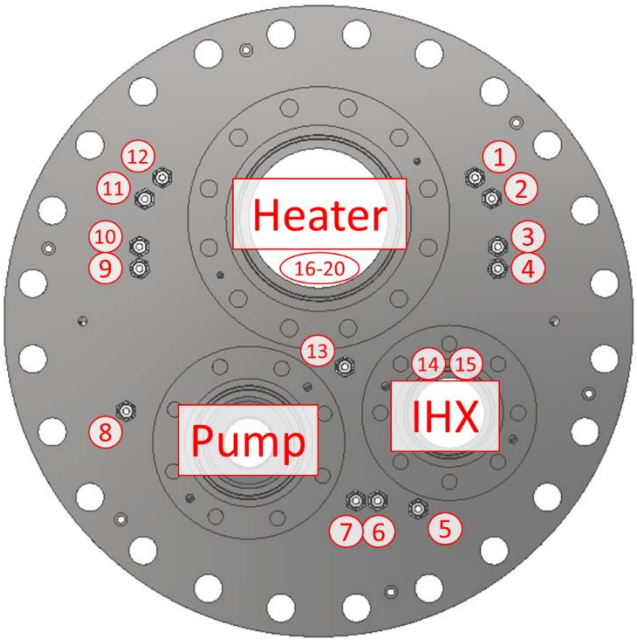

Figure 22: THETA instrumentation port locations

Port # 4, 6, and 9 possess 1/4" OD, 25-junction, k-type ungrounded thermocouple probes. The junctions possess a pitch of 2.375" and capture hot and cold pool axial temperatures with high fidelity, Figure 23.

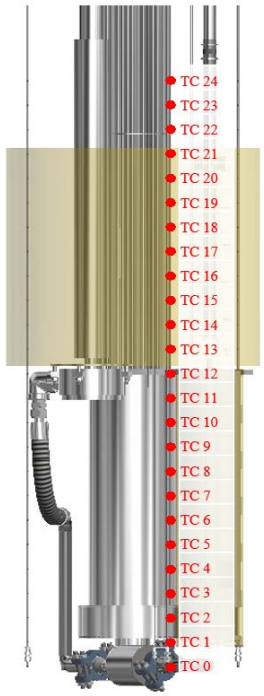

Figure 23: Multi-junction TC positions for ports 4, 6, and 9, hot pool sodium shown with translucent yellow for reference.

A photo of the multi-junction TC probes installed into ports 4 and 6 can be found in Figure 24. A photo of the three multi-junction TC probes in the cold pool region can be found in Figure 25.

Figure 24: Multi-junction TC probe installed in port #6, left. Multi-junction TC probe installed in port #4, right.

Figure 25: Dry fitting of THETA cold pool components in preparation for testing in deionized water. Multi-junction TC probes installed in ports # 4, 6, and 9 can be seen.

Optical fiber temperature sensors will be used to acquire distributed temperature data at spatial resolutions down to 0.65 mm and measurement rates of up to 250 Hz. These sensors are constructed from single mode silica fibers, Figure 26. An ODISI 6104 optical fiber interrogator system has been purchased and received from Luna Innovations, manufacturer specifications provided in Table 4.

.

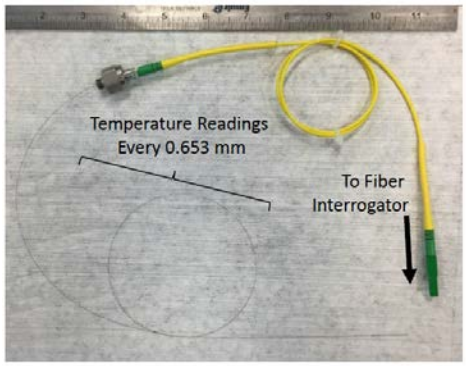

Figure 26: Photo showing 150 µm OD silica optical fiber

Table 4: ODISI 6104 spatial resolution and measurement rate

Spatial Resolution [mm]	Measurement Rate [Hz]
0.65	62.5
1.3	125
2.6	250

Optical fibers will be sheathed in a protective 1/16” OD 0.009” wall, 316 stainless steel capillary tube to protect them from sodium. Given there are no connection points for the 1/16” capillaries at the base of the 28” METL vessel, the optical fiber capillaries in ports 3, 7, and 10 will be mechanically attached to 1/4” multipoint thermocouple probes in ports 4, 6, and 9 to provide support, Figure 27 and Figure 28.

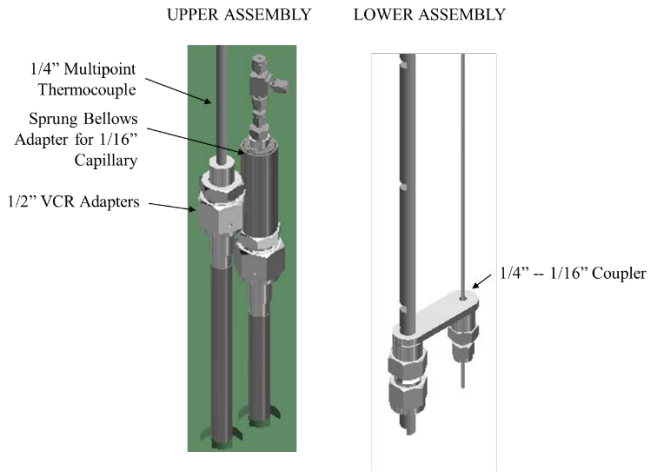

Figure 27: Optical fiber capillaries mechanically coupled to 1/4" multi-junction thermocouples

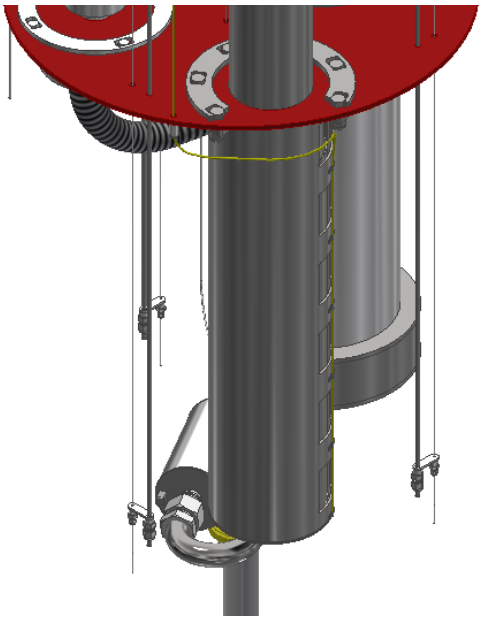

Figure 28: View of 3 optical fiber capillaries coupled to 1/4" multipoint thermocouple probes

A custom sprung bellows assembly has been designed to provide tension and to make up any thermal expansion differential between the 1/16" capillary tubes in ports 3, 7, 10, 13, and 14 and the rest of the primary vessel components, Figure 29. A complete description of the design can be found in [1]. A photo of the sprung bellows adapter installed in port #7 on the primary flange can be found in Figure 30.

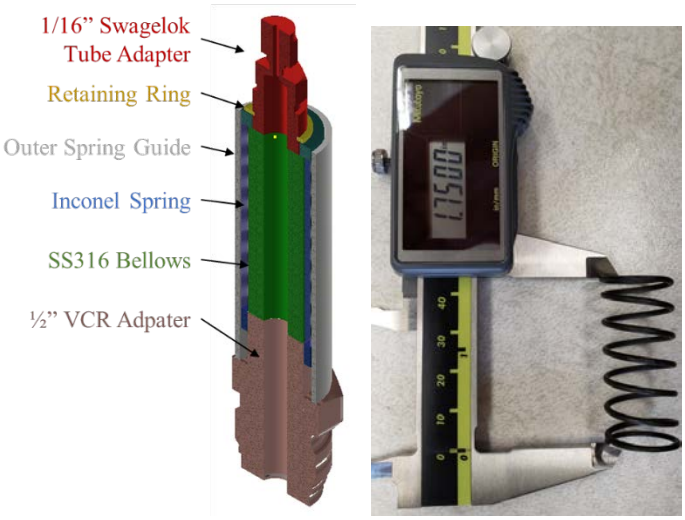

Figure 29: Sprung bellows to makeup thermal expansion differential of 1/16" capillaries, left. High temperature Inconel spring photo, right.

Figure 30: Sprung bellows adapter installed in port #7

3.3. Intermediate Heat Exchanger

An intermediate heat exchanger (IHX) has been designed to transfer heat from the THETA primary sodium to its secondary sodium system. As can be seen in Figure 31, the current design is a shell and tube type, with primary sodium on the shell side, and secondary sodium that flows through a tube bundle up-comer. Baffles with a ~1/2 shell window cross section are used to promote thermal mixing in the primary sodium. The down-comer sodium on the secondary side flows through a vacuum insulated tube. This is representative of typical SFR designs where the coldest sodium is delivered to the bottom of the intermediate heat exchanger to provide a counter-flow heat exchange. Two expansion bellows on the downcomer tube, one in the vacuum region and one above the vacuum region, accommodate thermal expansion differentials in the IHX. The design facilitates a 1/2" rod running concentric down the length of the shell to allow for adjustment of the IHX primary sodium outlet elevation into the cold pool, as will be discussed in a later section.

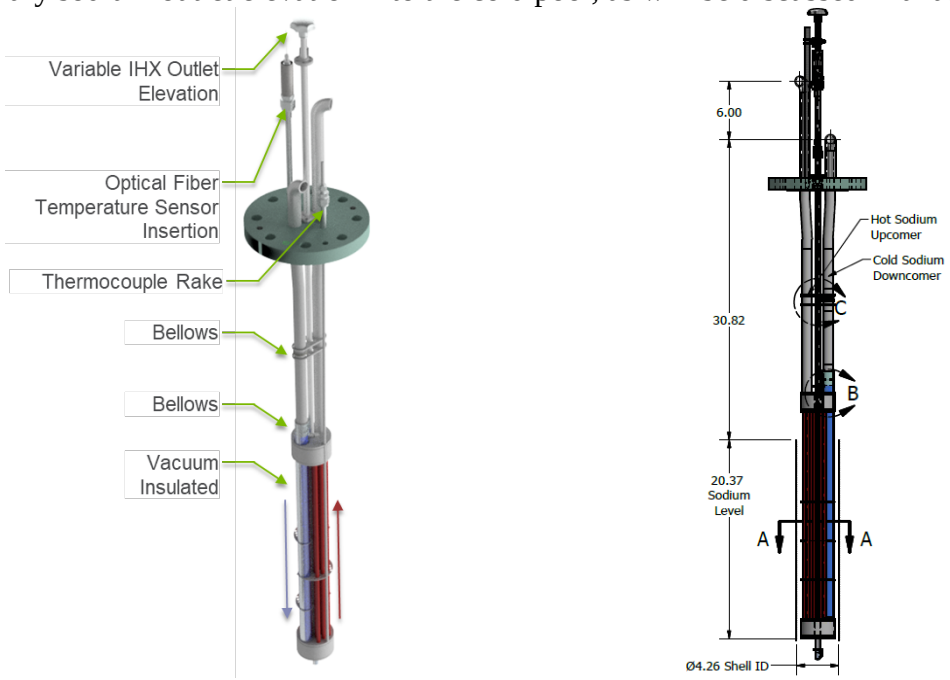

Figure 31: Shell and tube intermediate heat exchanger

Figure 32: Drawings showing IHX baffle plate and tube bundle upcomer

The heat exchanger was sized using the effectiveness-NTU method for one shell pass and a tube bundle pass. This method identifies the maximum possible heat transfer rate and uses a calculated effectiveness to determine the actual heat transfer rate, Eq. 1.

$$\dot{q} = \varepsilon \dot{q}_{max} \tag{1}$$

The effectiveness for a heat exchanger of this type as a function of transfer units and capacity ratio can be found in Eq. 2.

$$\varepsilon = \begin{cases} \dfrac{1 - \exp\left[-NTU\,(1 - C_R)\right]}{1 - C_R \exp\left[-NTU\,(1 - C_R)\right]} & \text{for } C_R < 1 \\ \dfrac{NTU}{1 + NTU} & \text{for } C_R = 1 \end{cases} \tag{2}$$

Where C_R is a dimensionless number referred to as the capacity ratio, comparing the capacitance rates of the tube and the shell side fluids, Eq. 3, and NTU is the number of transfer units, calculated using Eq. 4.

$$C_R = \frac{\dot{C}_{min}}{\dot{C}_{max}} \tag{3}$$

Where $\dot{C}_{min}$ and $\dot{C}_{max}$ are the minimum and maximum of the capacitance rates of fluid on either side of the heat exchanger.

$$NTU = \frac{UA}{\dot{C}_{min}} \tag{4}$$

The conductance of the heat exchanger, UA, is a function of both geometry and heat transfer in the heat exchanger. The conductance may be found by taking the inverse of the total thermal resistance, Eq. 5.

$$UA = \frac{1}{R_{tot}} = \frac{1}{R_{h,tube} + R_k + R_{h,shell} + R_f} \tag{5}$$

Where $R_{h,tube}$ is the convection resistance from the tube fluid to the tube inner wall, R_k is the resistance to conduction in the tube wall, $R_{h,shell}$ is the convection resistance from the shell fluid to the tube outer wall, and R_f is the resistance due to fouling. According to literature the fouling resistance in alkali metal heat exchangers is negligible if oxide level is kept below a few wppm [3]. The convection resistance may be determined with the use of the Nusselt number. On the tube side, the Nusselt number was found using a correlation for NaK flowing through a tube [4], Eq. 6.

$$Nu = 4.82 + 0.0185 \cdot Pe^{0.827} \tag{6}$$

On the shell side, the Nusselt number was found using a correlation for in-line flow through un-baffled rod bundles in wide spaced arrays (tube pitch / tube diameter = P/D > 1.35) [5], Eq. 7. Note that P/D for the above THETA IHX is 1.73.

$$Nu = 6.66 + 3.126\frac{P}{D} + 1.84\left(\frac{P}{D}\right)^2 + 0.0155(\bar{\varphi}Pe)^{0.86} \quad (7)$$

Where $\bar{\varphi}$, the ratio between eddy diffusivities of heat and momentum, is generally assumed equal to one [6].

Using the thermal hydraulic parameters given in Table 5, the performance of the THETA IHX may be predicted. As can be seen, the secondary sodium system flowrate was set to 5 GPM, the primary sodium inlet temperature was set to 550 °C, the secondary sodium inlet temperature was set to 450 and 500 °C. The shell side temperature differential and thermal power dissipation as a function of shell side flow rate can be found plotted in Figure 33.

Table 5: Intermediate heat exchanger sizing parameters

Parameter	Value	Unit
$Q_{sodium,secondary}$	5	GPM
$T_{sodium,primary,in}$	550	°C
$T_{sodium,secondary,in}$	450, 500	°C

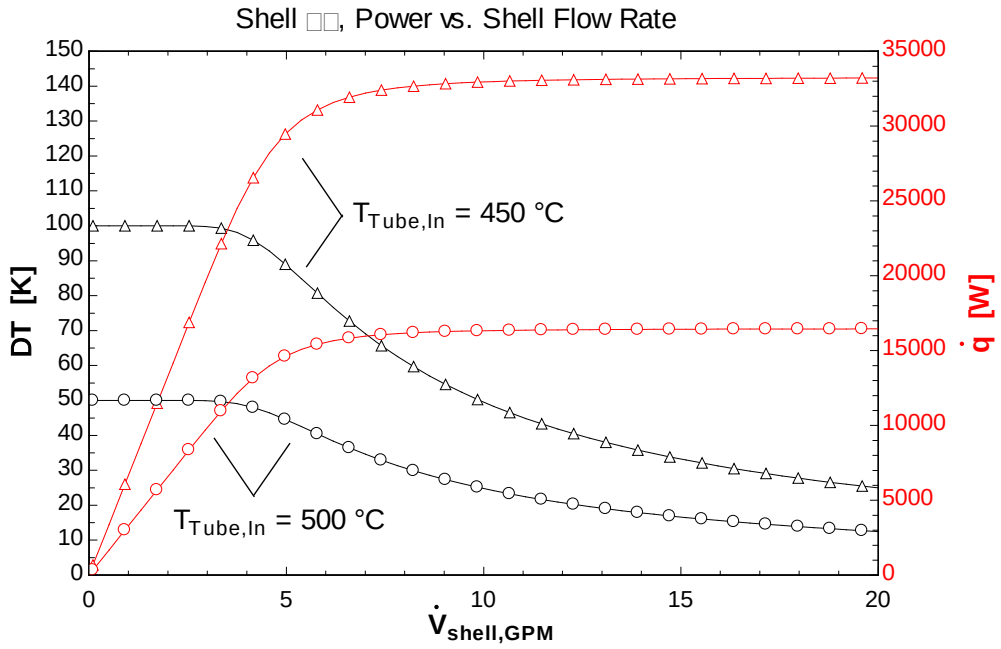

Figure 33: IHX predicted shell side temperature differential and thermal power dissipation as a function of shell side flow rate

The IHX possesses a variable height outlet mechanism allowing for exiting of cold sodium at various elevations in the cold pool to study the transient and steady state temperature profile which develop throughout an SFR as a result of changing this variable, Figure 34. Depositing cold sodium

at a lower elevation in the cold pool is predicted to result in more stratification and ultimately result in a more thermally stratified hot pool. This will be an important variable to study for the development of reactor codes. Figure 35 shows drawings of the inner and outer barrel. As can be seen there are qty. (6) 2.75” square windows at elevations spaced 4.5” apart from center to center. The inner barrel rests on a stainless steel cone on the bottom of the outer barrel in a Hastelloy C-276 seat, reducing the likelihood of galling. A photo showing the finished IHX outlet inner and outer barrel can be seen in Figure 36. The IHX outlet can be seen installed onto THETA in Figure 21.

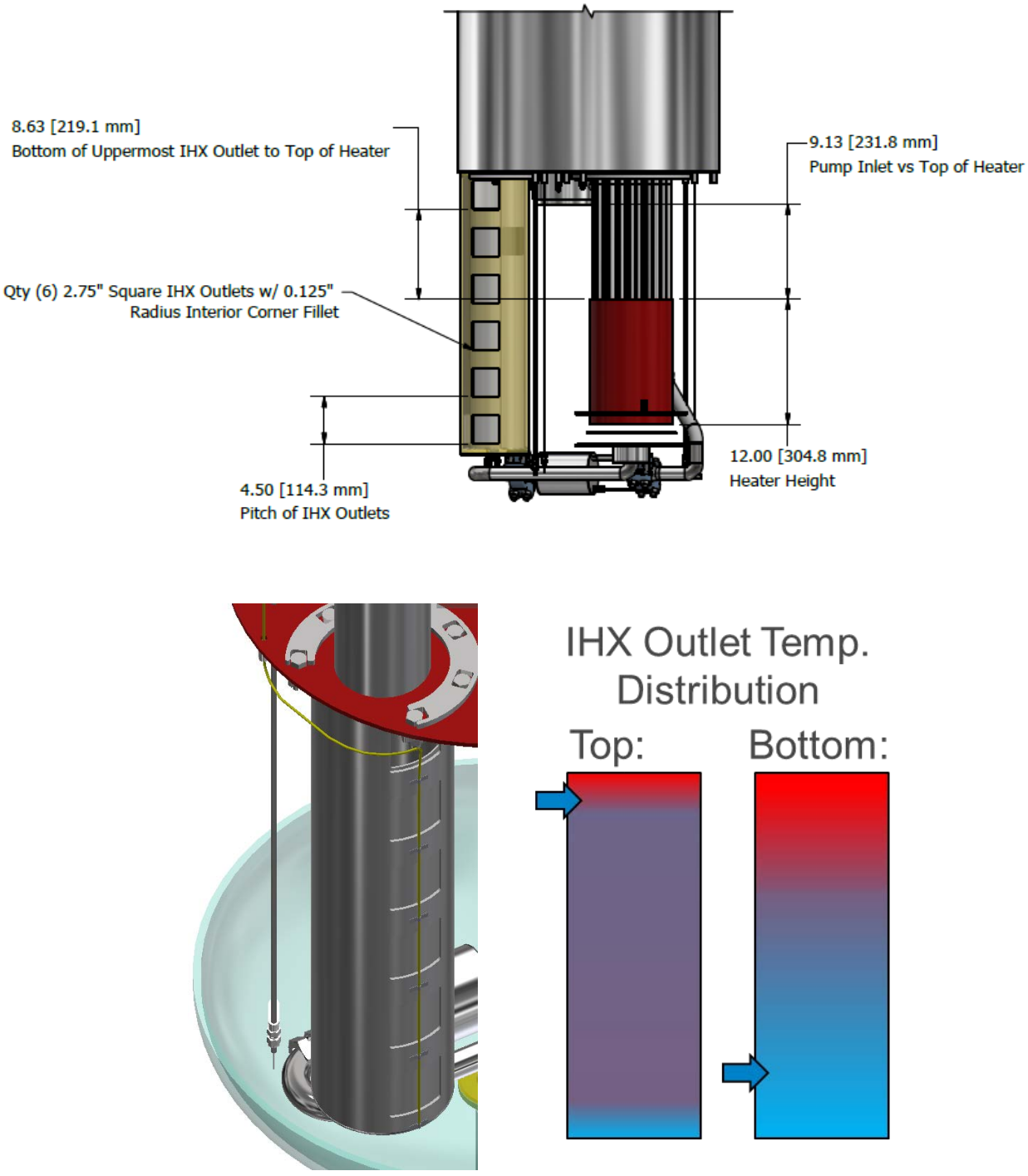

Figure 34: IHX Outlet dimension, top. Isometric model of variable elevation IHX outlet, bottom left. Drawing showing predicted cold pool temperature distribution as a function of IHX outlet window elevation, (red = hot, purple = warm, blue = cold), bottom right.

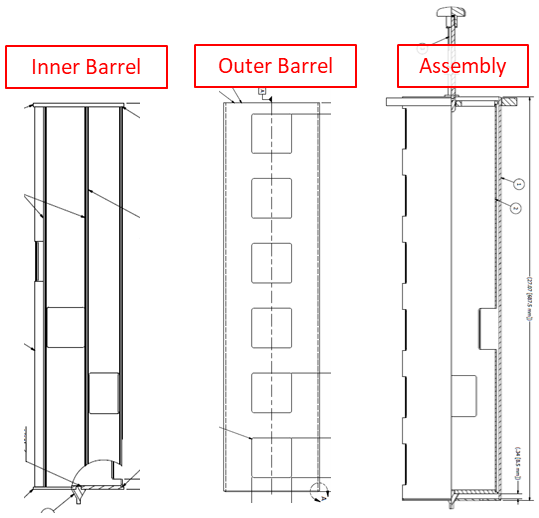

Figure 35: Variable elevation IHX outlet. Drawings showing the inner barrel, left, outer barrel, middle, and the assembly of inner/outer barrel and actuator stem, right.

Figure 36: Photo showing the IHX outlet inner barrel, left, and the outer barrel, right

3.4. Submersible Flowmeter

A submersible permanent magnet flowmeter has been designed to acquire primary sodium flowrate, Figure 37. The flowmeter uses a magnetic field generated by high temperature Samarium-Cobalt (SmCo) magnets, oriented perpendicular to sodium flow, to generate a Lorentz current that is linearly proportional to flow. A complete description of the design and construction of the flowmeter can be found in [1]. A photograph of the completed flowmeter can be found in Figure 38. Flowmeter calibration in a sodium loop was completed, a photo of the flowmeter installed in series with a reference flowmeter can be found in Figure 39.

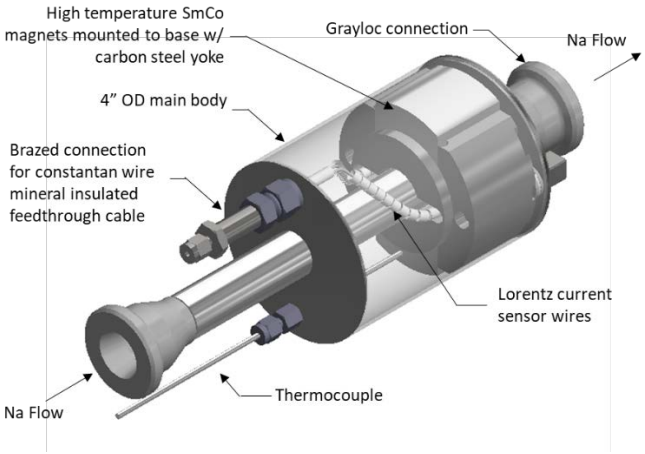

Figure 37: Submersible permanent magnet flowmeter

Figure 38: Photo of the THETA submersible permanent magnet flowmeter

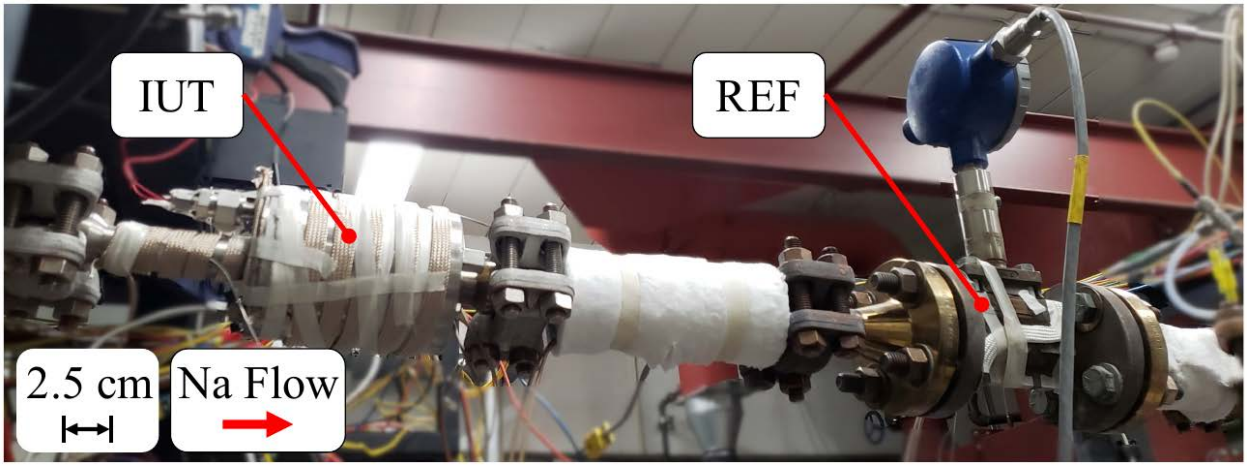

Figure 39: Flowmeter calibration against in-line reference meter. Instrument Under Test (IUT) is THETA flowmeter with 2X pre-heating tape heater zones installed. The Reference (REF) meter is a Foxboro M83, 1" nominal size vortex shedder flowmeter, (PN: 83F-T01S2STRJA-G).

The flow rate of the EM flowmeter may be calculated with Eq. 8

$$Q = C\,Q_{IUT} = C\frac{\pi V_m d}{4BK_B K_\rho K_S} \tag{8}$$

Where *Vm* is the measured voltage of the flowmeter, *d*, is the inner diameter of the flowmeter, *B* is the measured magnetic field, and the *K* factors are semi-empirical correlations that account for geometry and electrical affects particular to the flowmeter [7]. Q_{IUT} is the calculated flowrate and *C* is a calibration coefficient that is found after calibrating the meter against a master reference meter that possesses a NIST traceable certificate showing it complies with ANSI Z540-1-1994. The reference meter was a Foxboro M83 with a maximum rated temperature of 420 °C. Note that wetting was established by bringing the IUT up to 400 °C, then the measured voltage was monitored over a period of 2+ hours to ensure zero differential in measured voltage as a function of time, Figure 40. Figure 41 provides a plot of Q_{IUT} as a function of the master meter flowrate $Q_{REF,}$ found during calibration at 220 and 400 °C. The calibration coefficient was then calculated for the various flowrates and temperatures tested, Figure 42. Depending on the operating regime of the flowmeter, the calibration coefficient can vary slightly, from approximately 1.04 to 1.10. This is likely due to the magnetic field distortion as it is being dragged down the piping with the conductive flowing sodium. In order to account for this variation a power function may be used to calculate the calibration coefficient in real-time for a wide variety of operating regimes, Eq. 9.

$$C = 1.2475(Q_{IUT})^{0.0193} \tag{9}$$

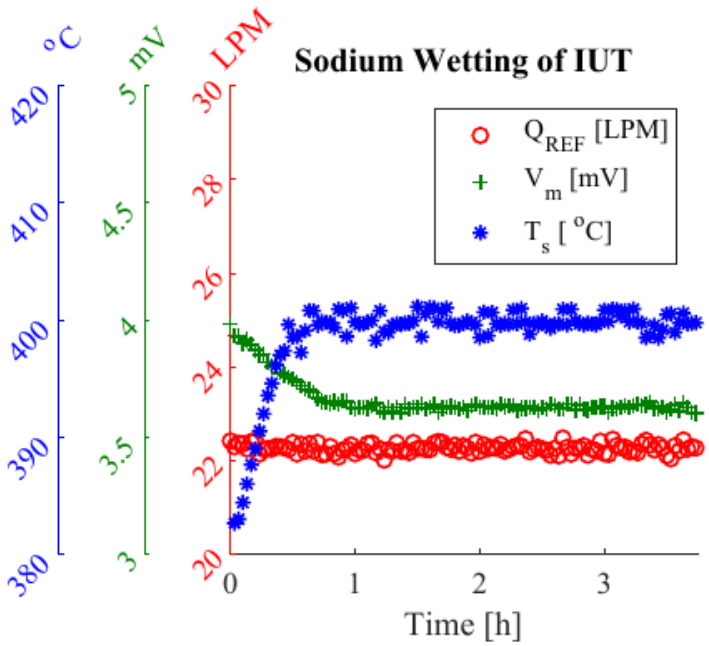

Figure 40: Wetting of IUT at 400 C and 22.4 LPM. As can be seen, there was no change in measured voltage for a period of >2.5 hours.

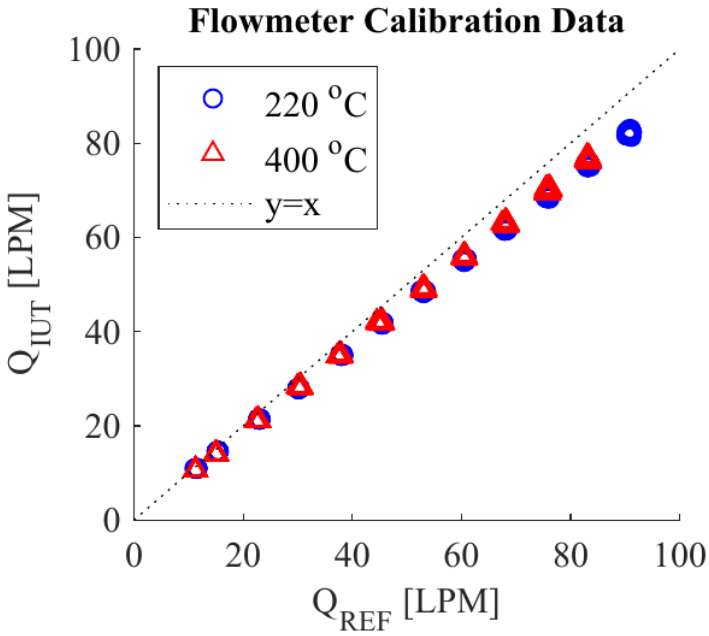

Figure 41: Flowmeter induced voltage vs flow rate for THETA submersible electromagnetic flowmeter, [1]. Error bars are smaller than plot markers. Error less than 3.5% over all flowrates and temperatures.

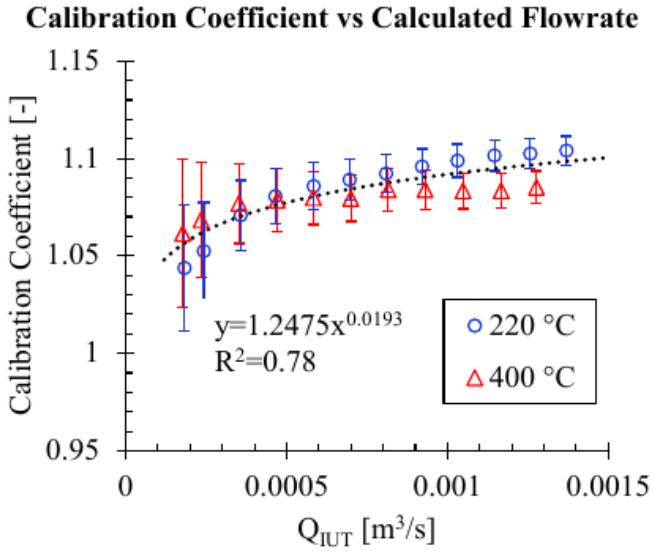

Figure 42: Calibration coefficient as a function of Q_{IUT}

3.5. Pump

The primary sodium centrifugal pump has been received from Wenesco Inc., Figure 43. The flow curve for the pump using deionized water can be found in Figure 44 [1].

Figure 43: Pump as delivered, left, 4.5" OD impeller, right.

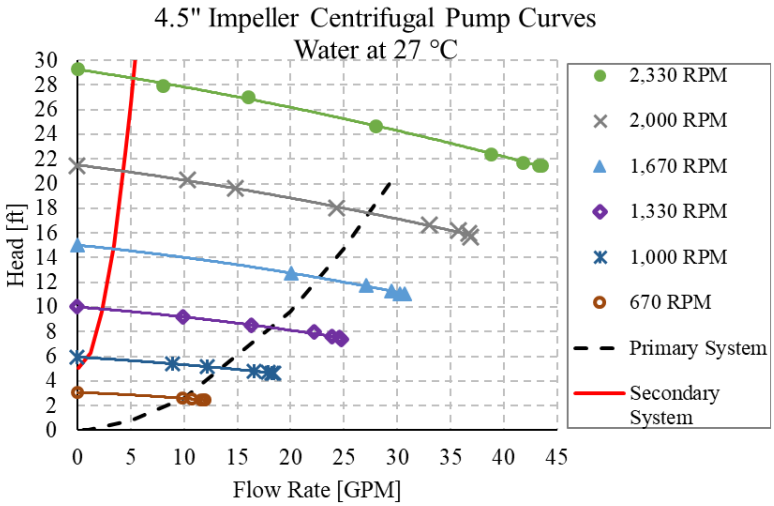

Figure 44: Pump curves made using water at 27 °C as surrogate fluid. System curves shown for primary and secondary sodium.

A photo of the air-to-sodium seal for the centrifugal pump shaft can be found in Figure 45. As can be seen it consists of a packing block that houses three layers of 1/2" square high speed packing cord made with expanded-graphite yarn with carbon yard corners. After installing the first layer of packing, a lantern ring is installed that acts to trap a layer of pressurized inert gas between the first layer and the second and third layers of packing, Figure 46 and Figure 47. This ensures a hermetic seal for the cover gas in the sodium as the inert gas void space provided by the lantern ring can be regulated at a slightly higher pressure than the sodium cover gas, limiting cover gas egress or air ingress into the system.

Figure 45: Photo showing the air-to-sodium seal for the THETA centrifugal pump. Shown from left to right: packing block, lantern ring, follower.

Figure 46: Photo showing the 5” 300# ANSI flange with graphite gasket in place in preparation for installation of packing block. Nitronic-60 helicoil thread adapters are installed in all threads to reduce likelihood of galling.

Figure 47: Photo showing the packing block cavity. On the right can be seen a single layer of graphite packing. Two holes are bored radially into the cavity, the lower one shown is for inert gas pressurization of the lantern ring void, the upper bore is for an 1/8” thermocouple to monitor packing temperatures during operation.

A debris 'thrower' is mounted below the pump flange on the shaft, Figure 48. This thrower catches any graphite debris that may be shed from the seal above. As the shaft spins, the debris is deposited into a debris well below, Figure 49, Figure 50.

Figure 48: Photo showing the wetted face of the pump flange along with the thrower that acts to centrifugally deposit debris falling from the packing block into the debris well. Also notice the ethanol, this is sprayed onto lint-free lab wipes and used to ensure cleanliness of all components before testing.

Figure 49: Photo showing the 5" 300# mounting flange on the THETA primary flange. The energized spring seal groove can be seen on the raised face. A debris well can be seen which acts to catch any dust or large particles that may fall from the graphite packing seal.

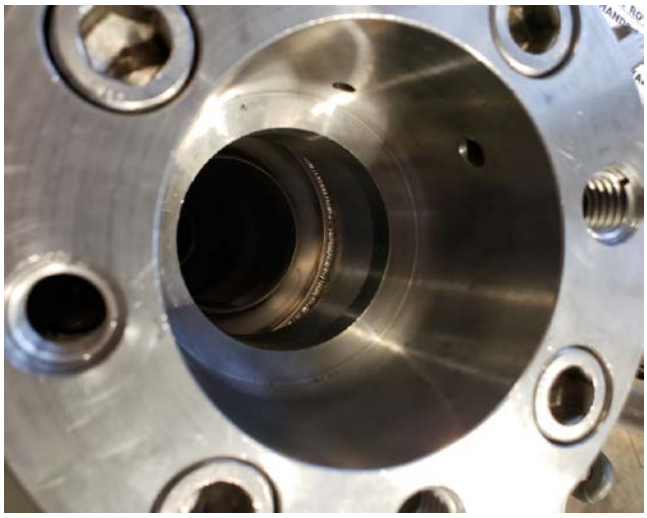

Figure 50: Photo showing the packing block installed with the debris well below.

A labyrinth seal consisting of a bottom plate that is sandwiched between the case and the inner vessel and a shaft adapter was added to reduce flow from out of the top of the pump case, Figure 51 and Figure 52. The pump shaft does not possess a lower bearing; thus a contact free seal is required to reduce unwanted sodium egress out of the top of the case, into the hot pool. The labyrinth seal works by introducing a serpentine path which increases the pressure differential, thus reducing flow.

Figure 51: Photo showing the centrifugal pump case with labyrinth seal lower plate and shaft adapter.

Figure 52: Photo showing the labyrinth seal shaft adapter

The assembled pump was installed on to the primary vessel, Figure 53, and labyrinth seal and impeller installed onto the bottom of the shaft afterwards, Figure 54. Figure 55 shows the completed lower pump assembly with case and piping installed.

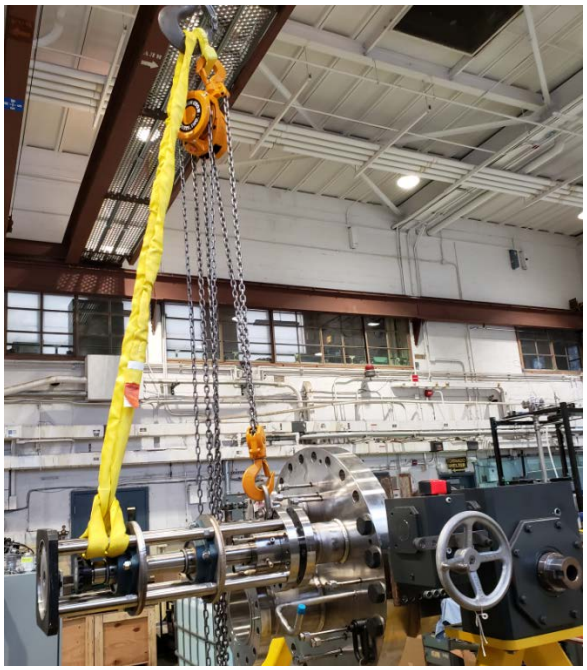

Figure 53: Photo showing the installation of the centrifugal pump shaft and upper bearing assembly into THETA.

Figure 54: Photo showing the bottom side of the inner vessel, pump case is not installed so the labyrinth plate and pump impeller are visible

Figure 55: Photo showing the underside of the inner vessel with pump case and piping installed

Colleagues at Oak Ridge National Laboratory have 3D printed a 316L pump impeller that will be tested in the future on THETA to assess the long term reliability of this technology in a critical sodium component, Figure 56 [8].

Figure 56: 4.5" Diameter 316SS 3D printed impeller by Oak Ridge National Laboratory, [8]

3.6. Immersion Heater

The immersion heater and associated electrical enclosure have been received from Chromalox, Figure 57. Heater elements were tested with a multimeter to ensure proper rated resistance of ~35 ohms, indicating no significant damage occurred during shipment. The immersion heater is currently installed on the THETA primary flange, Figure 58. A photo showing one of four over temperature thermocouples welded to the Incoloy sheath. A process control thermocouple, not shown, is located at the center of the bundle. A photo showing the immersion heater shroud, which surround the heater to form the core, can be found in Figure 60. A photo showing the heater control panel on can be seen in Figure 61.

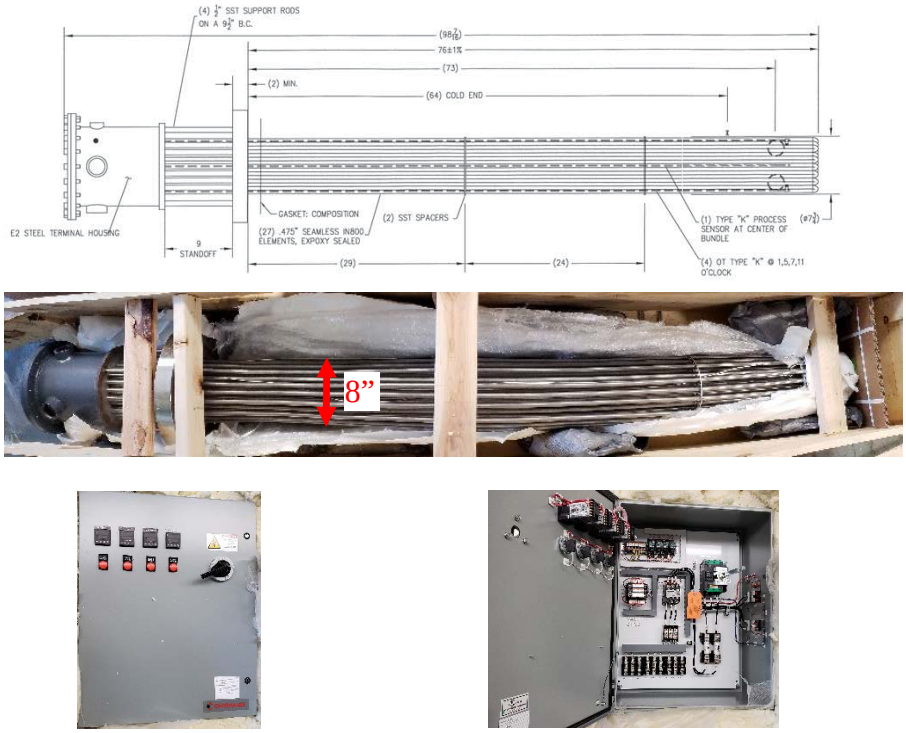

Figure 57: Chromalox 38 kW Immersion Heater (top). Heater control system electrical enclosure (bottom).

Figure 58: Photo showing the installation of the THETA immersion heater.

Figure 59: Photo showing two of the four thermocouples welded to the hairpin heaters at the bottom of the immersion heater

Figure 60: Photo showing the shroud that surrounds the immersion heater in the cold pool to form the core flow path

Figure 61: Photo of immersion heater control system online

4. Secondary Sodium Component Summary

This section provides an update for the THETA secondary sodium components and piping. A 3D isometric drawing of the current secondary system design can be found in Figure 62. As can be seen an AC Conduction based electromagnetic pump pushes sodium through an air-to-sodium heat exchanger, a permanent magnet flowmeter, and an intermediate heat exchanger.

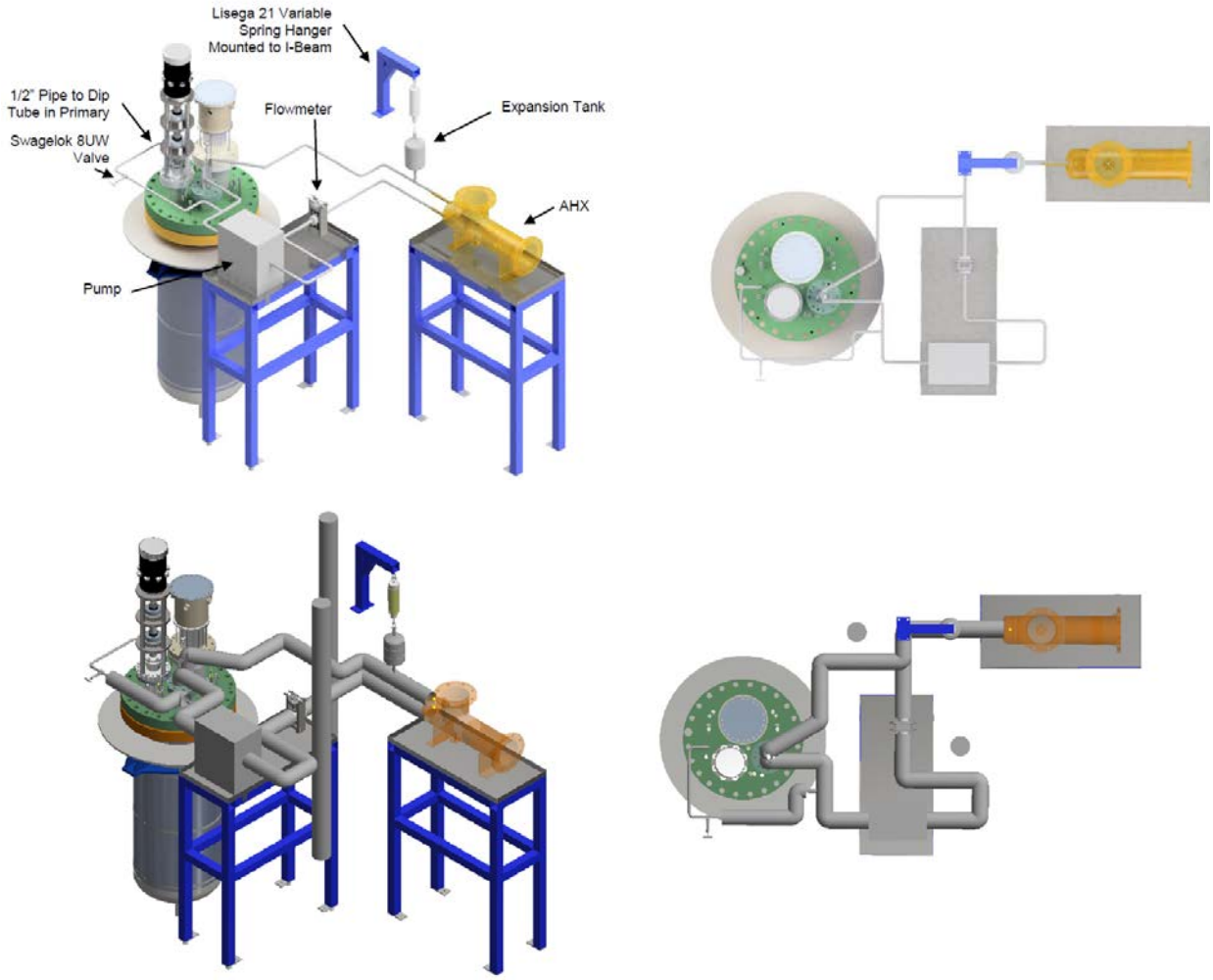

Figure 62: Isometric 3D drawing showing THETA secondary system without (top) and with (bottom) 2" of insulation

4.1. Sodium-to-Air Heat Exchanger

A custom, U-stamped (ASME BPVC Sec. VIII Div. 2) sodium-to-air heat exchanger was constructed at Enerquip LLC in Medford, Wisconsin. The heat exchanger is a tube and shell design, with sodium flowing through qty. (24), 0.75" OD x 0.049" wall, 24" long single pass seamless 316/316L SS U-tubes. The heat exchanger bonnet, tube sheet, tubes, and shell were fully welded with RT1 radiography, hydrostatic pressure test, and helium leak check to ensure no egress

of sodium during operation. The heat exchanger is rated for a maximum sodium temperature of 538 °C (1000 °F) at 100 PSIG with a maximum heat dissipation of 39 kW (133.8 kBtu/hr).

A photo of the sodium-to-air heat exchanger can be found in Figure 63. A summary of the heat exchanger sizing analysis from the manufacturer has been provided in Table 6.

Figure 63: Photo of the sodium-to-air heat exchanger as received from the manufacturer

Table 6: Sodium-to-Air heat exchanger specification sheet

HEAT EXCHANGER SPECIFICATION SHEET — Page 1 — **US Units**

Job No.			
Customer	Argonne National Laboratory	Reference No.	Matt Weathered
Address		Proposal No.	51156R2
Plant Location	Argonne, IL 60439	Date	5/31/19 Rev
Service of Unit	Cooler	Item No.	
Size	8.329 x 24 inch Type BEU Vertical	Connected In	1 Parallel 1 Series
Surf/Unit (Gross/Eff)	19.218 / 18.678 ft2 Shell/Unit 1	Surf/Shell (Gross/Eff)	19.218 / 18.678 ft2

PERFORMANCE OF ONE UNIT

Fluid Allocation		Shell Side		Tube Side	
Fluid Name		1200 SCFM Air		5 gpm Liquid Sodium	
Fluid Quantity, Total	lb/hr	5400.0		2102.0	
Vapor (In/Out)		5400.0	5400.0		
Liquid				2102.0	2102.0
Steam					
Water					
Noncondensables					
Temperature (In/Out)	F	77.00	180.12	1000.0	790.00
Specific Gravity				0.8262	0.8533
Viscosity	cP	0.0186	0.0212	0.2240	0.2670
Molecular Weight, Vapor					
Molecular Weight, Noncondensables					
Specific Heat	Btu/lb-F	0.2390	0.2416	0.3009	0.3055
Thermal Conductivity	Btu/hr-ft-F	0.0151	0.0176	36.044	39.482
Latent Heat	Btu/lb				
Inlet Pressure	psia	16.496		24.696	
Velocity	ft/sec	84.12		0.22	
Pressure Drop, Allow/Calc	psi	10.000	0.782	10.000	0.036
Fouling Resistance (min)	ft2-hr-F/Btu	0.00050		0.00200	

Heat Exchanged 133830 Btu/hr MTD (Corrected) 760.1 F
Transfer Rate, Service 9.43 Btu/ft2-hr-F Clean 20.50 Btu/ft2-hr-F Actual 19.39 Btu/ft2-hr-F

CONSTRUCTION OF ONE SHELL

Sketch (Bundle/Nozzle Orientation)

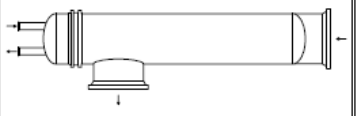

		Shell Side	Tube Side
Design/Test Pressure	psig	50.000 /	50.000 /
Design Temperature	F	250.00	1000.0
No Passes per Shell		1	2
Corrosion Allowance	inch	0.0000	0.0000
Connections	In inch	1 @ 8.0000	1 @ 1.0000
Size &	Out inch	1 @ 8.0000	1 @ 1.0000
Rating	Intermediate	@	@

Tube No. 22U OD 0.7500 inch Thk(Avg) 0.0490 inch Length 2.000 ft Pitch 0.9375 inch
Tube Type Plain Material SA-213 TP304L Tube (S) S30403 Tube pattern 60
Shell SA-312 TP304L Pipe (W) S30403 ID 8.3290 OD 8.6250 inch | Shell Cover (Integ.)
Channel or Bonnet SA-240 304L Pl. S30403 | Channel Cover
Tubesheet-Stationary SA-240 304L Pl. S30403 | Tubesheet-Floating
Floating Head Cover | Impingement Plate None
Baffles-Cross Type None %Cut (Diam) Spacing(c/c) 25.944 Inlet inch
Baffles-Long Seal Type None
Supports-Tube U-Bend Type None
Bypass Seal Arrangement 0 pairs seal strips Tube-Tubesheet Joint Expanded and seal welded (2 grooves)
Expansion Joint Type
Rho-V2-Inlet Nozzle 222.48 lb/ft-sec2 Bundle Entrance 0.00 Bundle Exit 0.00 lb/ft-sec2
Gaskets-Shell Side Tube Side
- Floating Head
Code Requirements ASME TEMA Class C
Weight/Shell 239.92 lb Filled with Water 337.60 lb Bundle 67.49 lb

Remarks (cont.) — Page 2

316/316L SA-213 seamless tubes. All 304/304L for remaining Tube Side Components
All 304/304L Shell Side Components
Industrial Finish: All surfaces are as machined or mill finish with welds cleaned to remove discoloration where accessible.

All Welded tubesheet and bonnet. Non removable.
NPS 300# ANSI Flange Tube Side Connections
NPS 150# ANSI Flange Shell Inlet
NPS 150# ANSI Flange Shell Outlet
NPT 3000# Coupling Shell Vent
U-Stamped
No China or India materials preferred. Acceptable from Japan, Europe, Canada, Domestic.
Passivation included

3.164 gallons for tubeside holdup

4.2. Secondary Sodium Piping

A thermal stress analysis was performed with CAESAR II computer software to ensure safe operation during all potential operating conditions. The piping analysis demonstrated passing of ASME B31.3 pipe code under all extreme and nominal operating conditions.

The secondary piping system is seamless 3/4" SCH 40 piping made with 316H stainless steel (ASTM 376 type 316H) given its superior strength at high temperature as compared to other grades of 300 series stainless. All of the fittings are 3/4" SCH 40 316/316L seamless tubes. Originally the fittings were specified as 316H, however during procurement it was found that these were not readily available from a domestic or DFARS (Defense Federal Acquisition Regulation Supplement) compliant supplier. 316/316L (ASTM A182 Type F316 or ASTM A403 Type WP316) possesses the same strength rating as 316H up to and including 1000 °F and is more readily available, therefore the fittings were specified using this grade of stainless.

The maximum temperature limit of the system is 538 °C (1000 °F) and the system has a design pressure of 50 PSIG. A total of six scenarios were identified for analysis to bound all possible operating conditions:

1. Filling system at 200 °C (392 °F)
2. System at maximum temperature, all piping and vessel at 538 °C (1000 °F)
3. IHX and AHX on, cold leg pump direction, 421 °C (790 °F) to 538 °C (1000 °F) ΔT
4. IHX and AHX on, hot leg pump direction, 421 °C (790 °F) to 538 °C (1000 °F) ΔT
5. Cold condition, system at 32 °C (0 °F)
6. Scenario #2 with seismic analysis

A screenshot of the CAESAR-II software setup to test Scenarios 1-6 can be found in Figure 64.

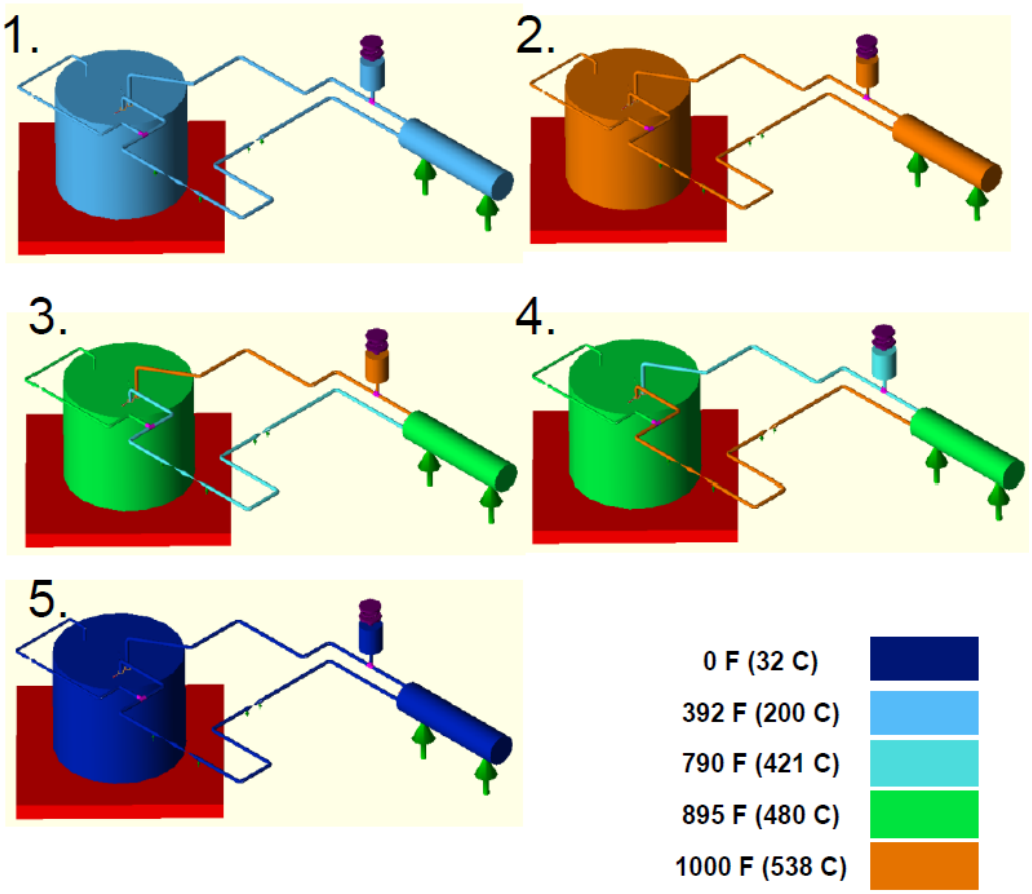

Figure 64: CAESAR operating scenarios showing vessel, AHX, expansion tank, piping temperatures

5. WATER TESTING

Water has been shown to be a good surrogate for sodium when performing thermal hydraulic experiments, possessing very similar density and viscosity to within an order of magnitude. In fact, water possesses some favorable characteristics over sodium when simulating certain thermal hydraulic phenomena with a small scale experiment; water has a reduced thermal conductivity resulting in a larger Pe number for a small scale experiment, allowing for more representative temperature gradients when simulating thermal stratification in a pool type SFR [9]. All of the THETA components will function in water except for the electromagnetic flowmeter. Therefore, the flowmeter described in Section 3.4 has been replaced with a Blancett B110-875, 3-30 GPM turbine mechanical flowmeter.

A 36” diameter, 60” tall, 260 gallon polypropylene vessel (PN: Chem-Tainer TC6330AB) was acquired for water testing of THETA, Figure 65. The vessel has a maximum temperature limit of 100 °C. A dip tube constructed with PVC supplies water and will drain water from the vessel with a self-priming pump assembly, Figure 65. The self-priming pump is a 1/3-HP centrifugal pump

with 41 ft max head (PN: Dayton 5GUP0). All wetted materials in the pump are compatible with deionized water (stainless steel, viton, carbon, ceramic). A 275 gallon intermediate bulk container is used to store the deionized water, Figure 66. The valve manifold shown in Figure 67 makes the water transfer a closed system, allowing the user to select water flow to or from the test vessel, thus conserving the deionized water between tests if the experiment must be drained, and reduces the chance of a gross leak of water.

Figure 65: 260 gallon polypropylene vessel for THETA water testing, left. Dip tube for transferring DI water between the intermediate bulk container and the polypropylene vessel, right.

Figure 66: 275 gallon intermediate bulk container of deionized water, left. Self-priming pump and valve manifold for transferring water between the intermediate bulk container and the test vessel.

In order to reduce biological (algae) growth in the deionized water, a UV filtration system was built. The manifold shown in Figure 67 attaches to the line from the intermediate bulk container and allows the user to throttle the water flow down to 6 GPM to expose the DI water to the UV lamp for sanitization.

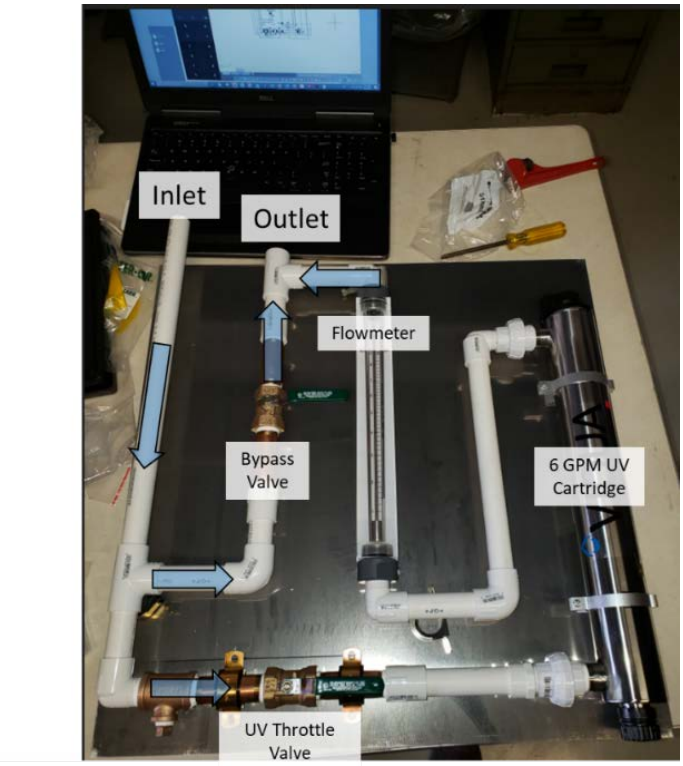

Figure 67: Manifold for ultraviolet sanitization of DI water to eliminate biological contamination. Water may be directed and through the UV cartridge with the UV Throttle Valve. The valve may be throttled to <=6GPM to ensure sufficient residency time of the flowing water to eliminate contaminates. A 0-10 GPM flowmeter is positioned in line with the UV cartridge circuit.

A Blancett B110-875, 3-30 GPM turbine mechanical flowmeter was installed in the system to acquire water flowrate, Figure 68. Photographs in Figure 69 show THETA installed on the yellow A-frame test stand and surrounded by a polypropylene vessel with multi-junction thermocouple probes plugged into gray umbilical boxes that feed data back to the data acquisition system. Also found in Figure 69 is a photo of the completed UV water sanitization system.

A pump shakedown has been performed of the assembled THETA, a plot showing flowrate as a function of pump speed can be found in Figure 70. The multi-junction thermocouple probes that acquire distributed temperature profiles in the hot and cold pool have all be connected to the data acquisition system and are ready to collect water testing data once the immersion heater has been

put online. The immersion heater control box was mounted and accommodations have been made to provide power for the heater, final wiring of the immersion heater to the control panel was completed.

Figure 68: Photo of THETA bottom assembly ready for water testing, a Blancett PN B110-875 turbine mechanical flowmeter will be used for water testing, shown installed at the bottom with yellow colored waterproof data cable connected.

Figure 69: THETA installed in polypropylene vessel with all thermocouple instrumentation attached, left. Completed water UV purification system and 275-gallon intermediate bulk container, right.

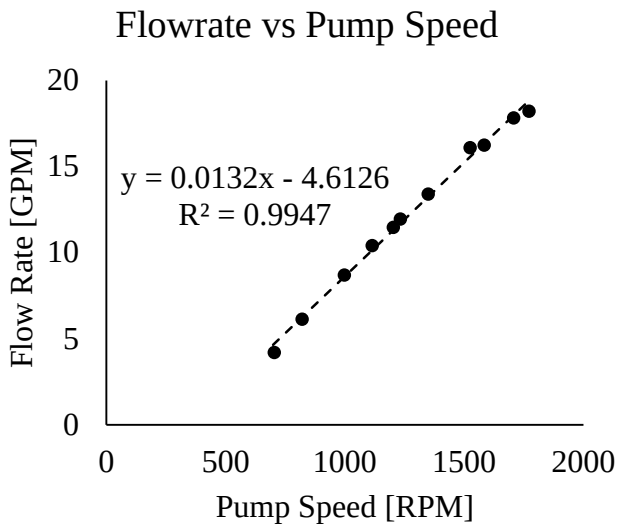

Figure 70: THETA pump shakedown preliminary results for flow rate as a function of pump speed. Water at room temperature (no immersion heater). Note that this data was taken without the shaft portion of the labyrinth seal installed, only the case lower plate portion, Figure 51.

A vibration sensor was attached to the pump above the experiment to provide feedback to the control system to emergency stop the heater and pump in case of extreme vibration, Figure 71. These vibrations are characteristic of the cantilevered shaft with high length to diameter ratio and occur due to a resonant frequency of the pump shaft, resonant 'swirling' of the pump impeller in the case, or a misalignment issue. Alternatively, a physical remote attached to an umbilical was made for the operator to be able to emergency stop the pump and/or heater in case of unexpected incident, Figure 72. These emergency buttons bypass any LabVIEW control and turn off their respective systems with a mechanical relay, avoiding a possible failure mechanism of LabVIEW freezing. A screenshot of the LabVIEW front panel used for water testing has been included in Figure 73 for reference. This program allows the operator to control the immersion heater 0-38 kW power input via SCR relay, turn on/adjust pump speed, read flowmeter/thermocouple data, as well as set data acquisition write-to-file parameters.

Figure 71: Photo of vibration sensor

Figure 72: Photo of SCRAM button

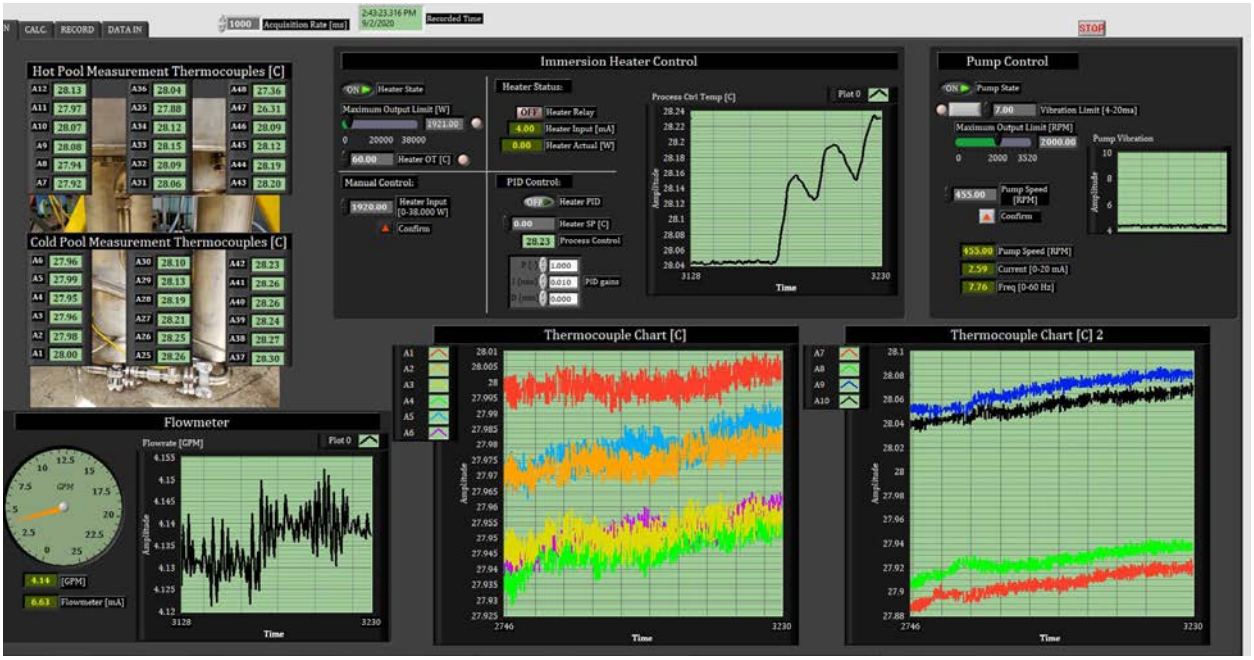

Figure 73: Screenshot of LabVIEW front panel used for THETA water testing data acquisition and process control

An experimental water testing campaign is underway, a summary of some of the more notable experiments can be found in Table 7. Figure 74-Figure 77 show tests that demonstrate the effect of varying the Reynolds number with constant Richardson number while varying the IHX outlet elevation. There seems to be identical normalized temperature distribution in the stratification effect when the Ri number is kept constant. Figure 78-Figure 85 show the effect of varying the Ri number while keeping the Re number constant. It is clear that a higher Ri number creates more thermal stratification, especially when the bottom IHX outlet (IHX = 1) is employed. Note, the locations of the thermocouples plotted in Figure 74 through Figure 85 can be found in Table 8.

Table 7: Thermo-hydraulic parameters for THETA water testing. The last column lists the IHX outlet window used (see Figure 34 - Figure 36) where window 1 is on the bottom of the cold pool and window 6 is on the top.

#	Power In [W]	Flow Rate [GPM]	Pump Speed [RPM]	Ri [Tanaka]	Re [Tanaka]	ΔT [C] (E-Balance)	IHX OUTLET - 1=btm
0902201	3750	5	540	11.58	2496	2.851	6
0902202	3750	5	540	11.58	2496	2.851	1
0902203	16843	8.25	840	11.58	4119	7.762	1
0902204	16843	8.25	840	11.58	4119	7.762	6
0903201	1626	5.007	525	5	2500	1.23	1
0903202	1626	5.007	525	5	2500	1.23	6
0903203	6504	5.007	525	20	2500	4.939	6
0903204	6504	5.007	525	20	2500	4.939	1
0904201	13008	5.007	525	40	2500	9.877	1
0904202	13008	5.007	525	40	2500	9.877	6
0904203	19513	5.007	525	60	2500	14.82	6
0904204	19513	5.007	525	60	2500	14.82	1

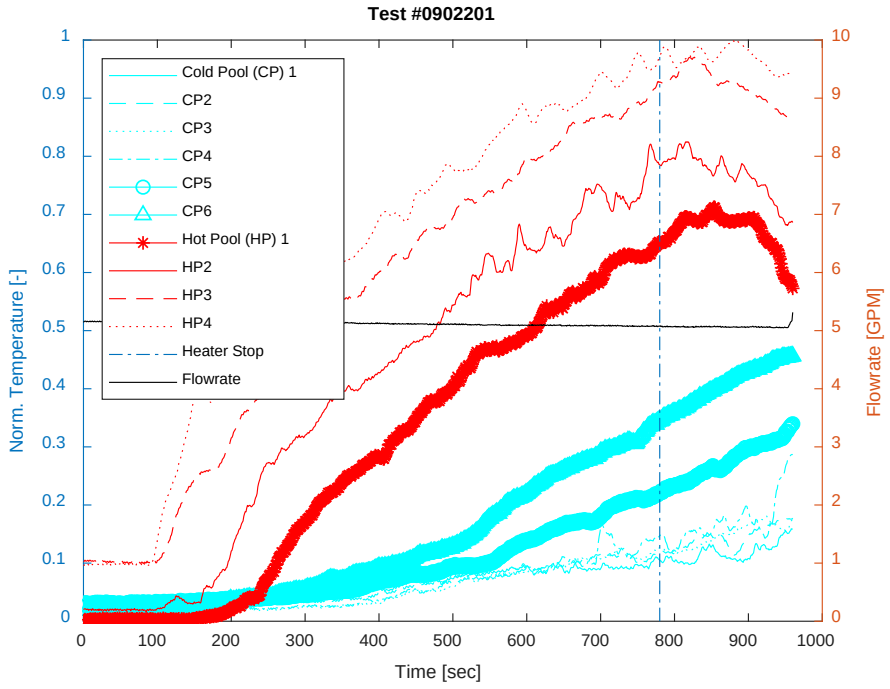

Figure 74: TEST # 0902201. Thermocouple Cold Pool (CP) 1 at base of cold pool with consecutive TCs spaced 4.75" up the pool. Thermocouple Hot Pool (HP) 1 at base of hot pool with consecutive TCs spaced 4.75" up the pool.

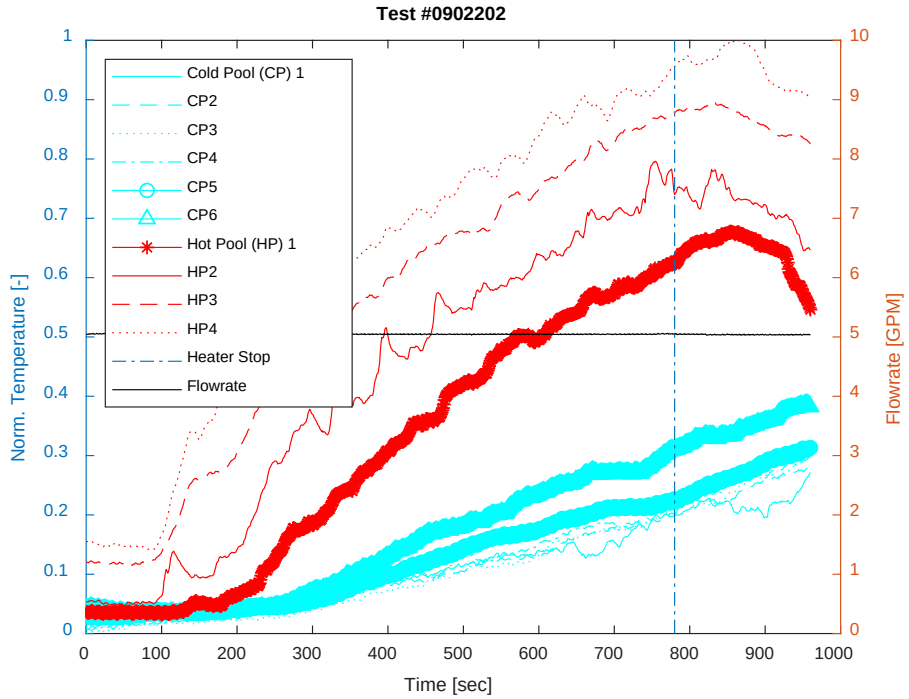

Figure 75: TEST # 0902202

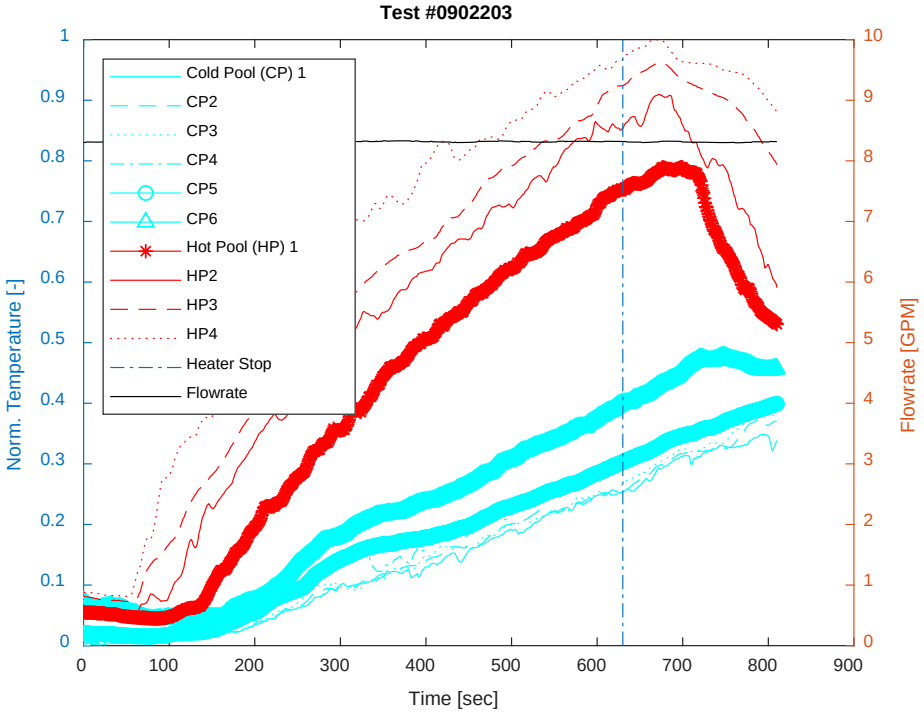

Figure 76: TEST #0902203

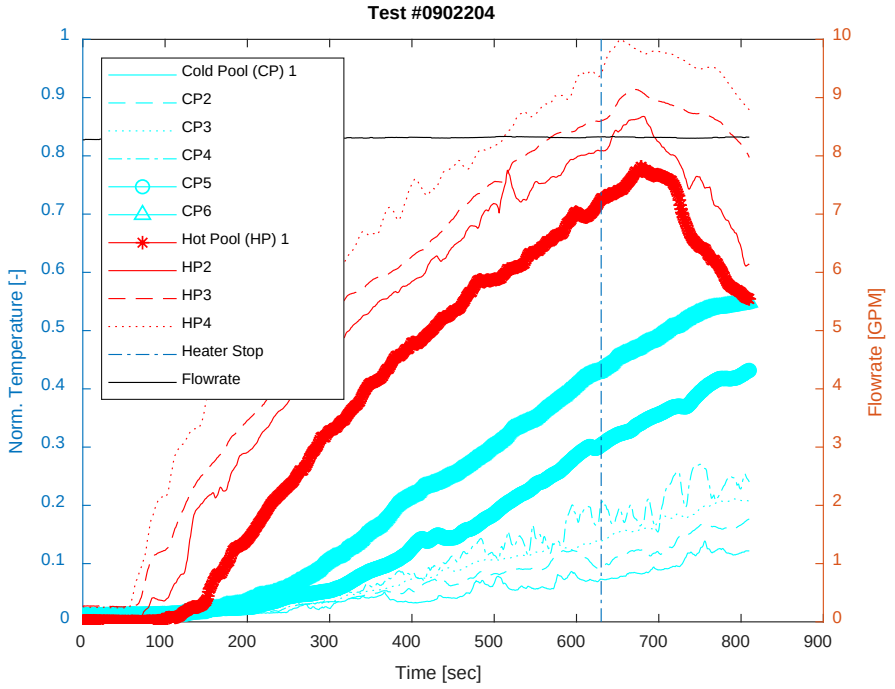

Figure 77: TEST #0902204

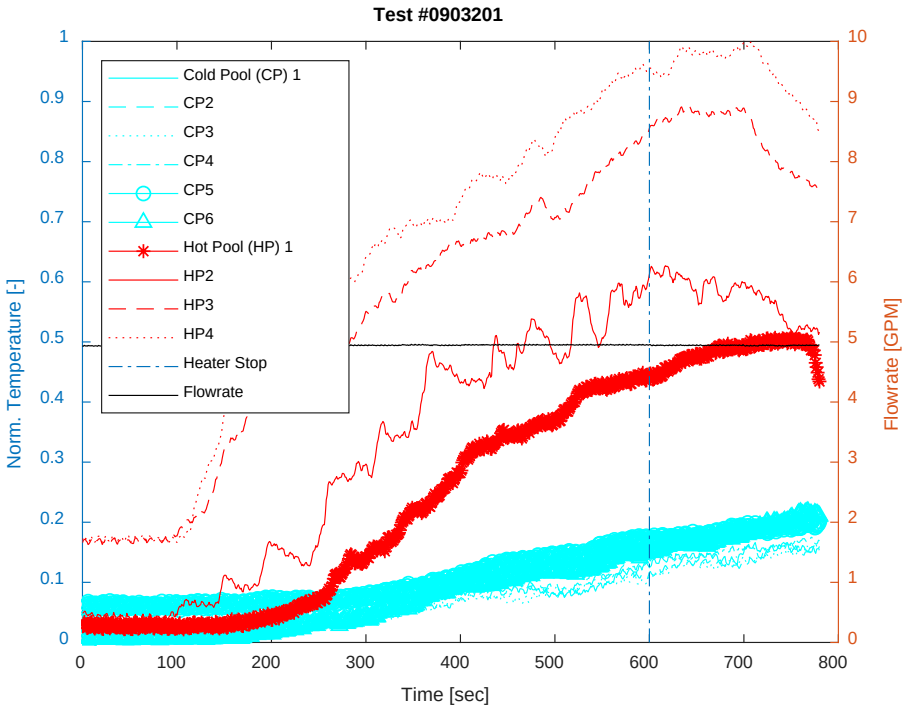

Figure 78: TEST #0903201

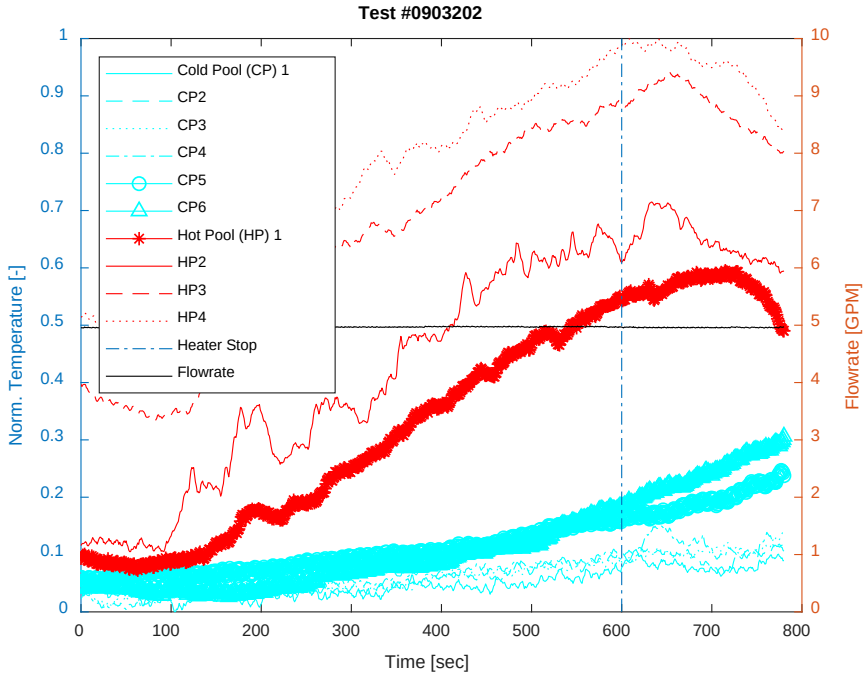

Figure 79: TEST #0903202

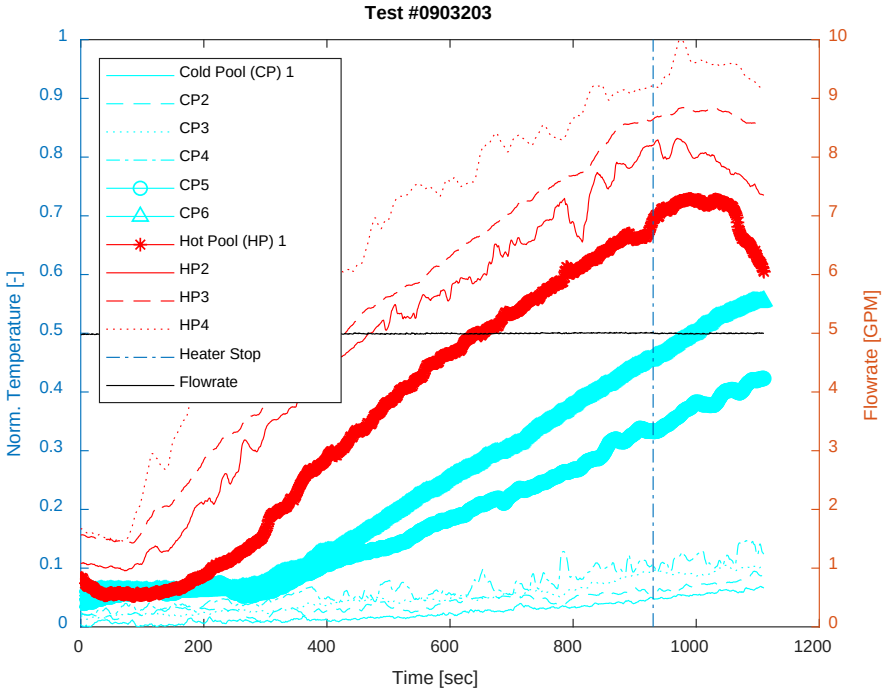

Figure 80: TEST #0903203

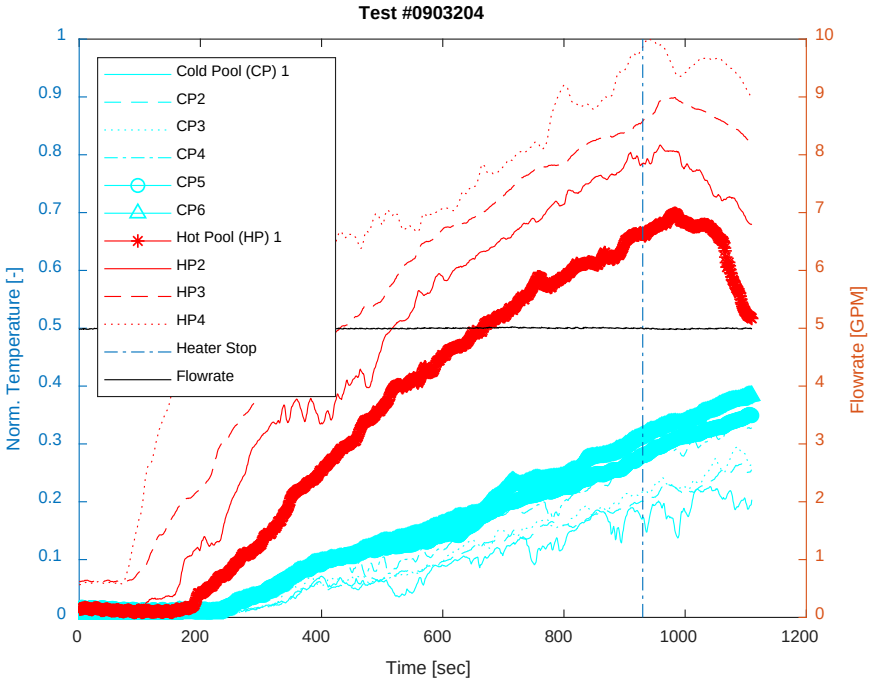

Figure 81: TEST #0903204

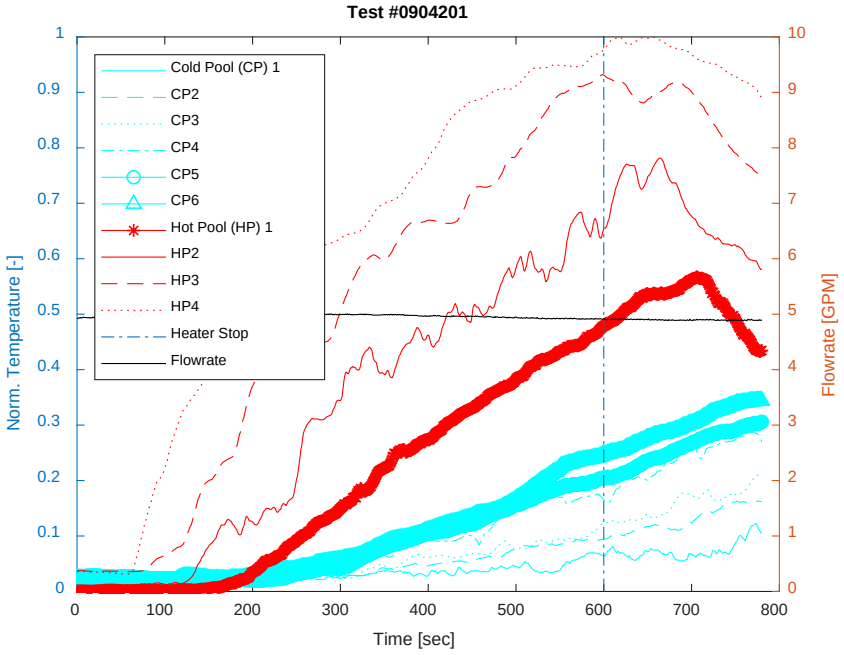

Figure 82: TEST #0904201

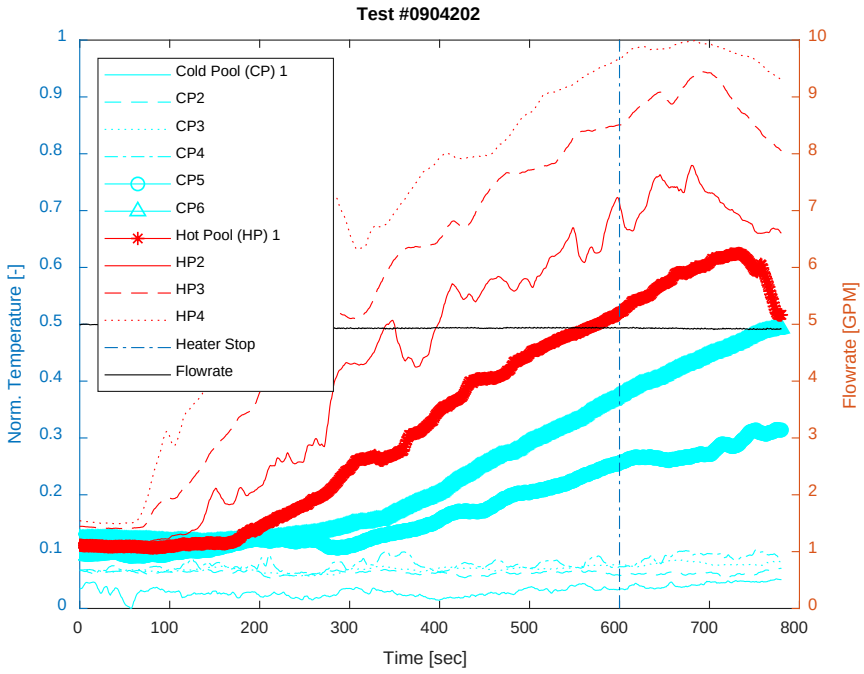

Figure 83: TEST #0904202

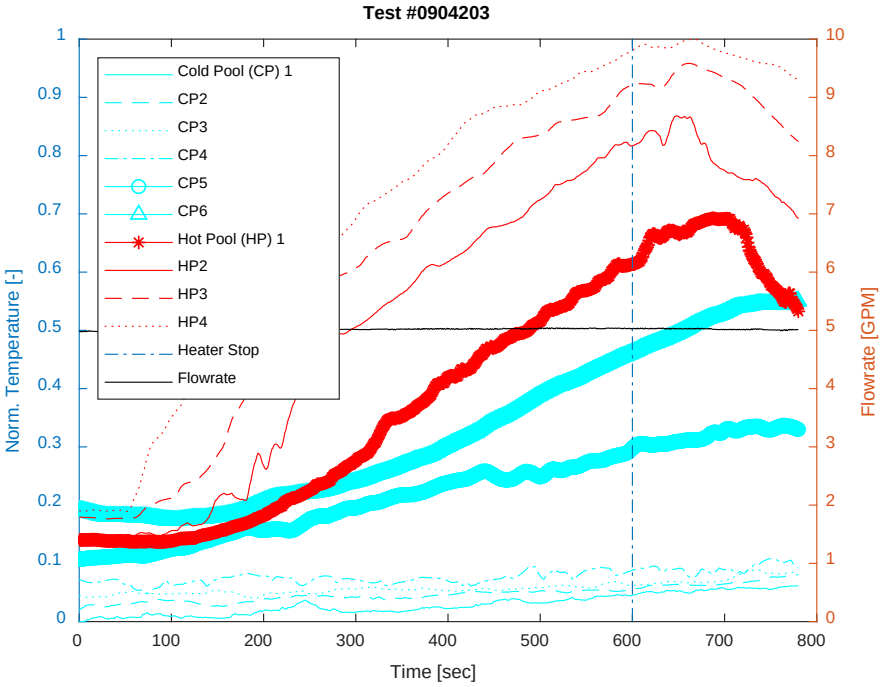

Figure 84: TEST #0904203

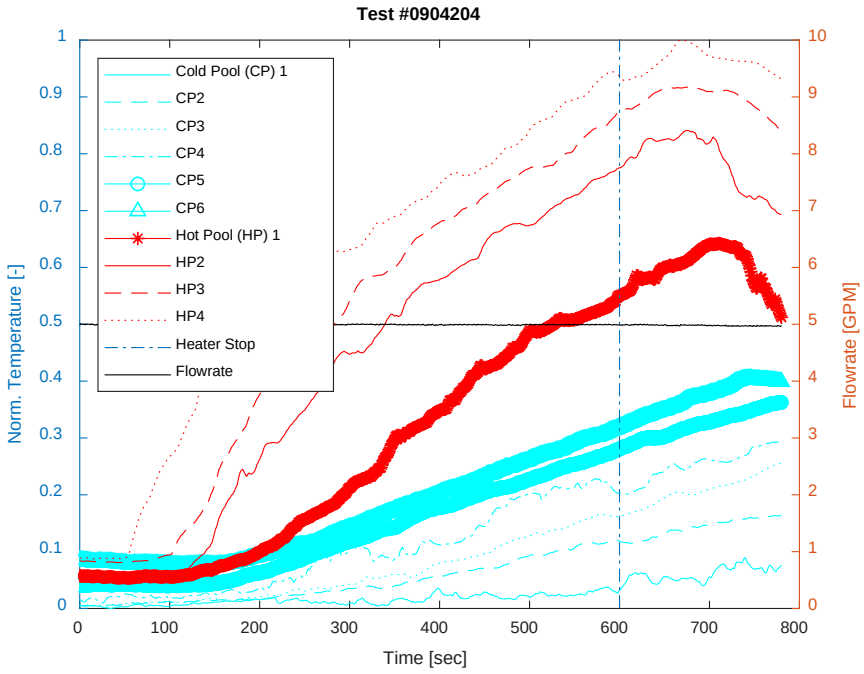

Figure 85: TEST #0904204

Table 8: Location of TCs in Figure 74 - Figure 85

TC	Location w/ Respect to Bottom of Inner Pool (Redan)
CP1	-62.9 cm (-24.75”)
CP2	-50.8 cm (-20.0”)
CP3	-38.7 cm (-15.25”)
CP4	-26.7 cm (-10.5”)
CP5	-14.6 cm (-5.75”)
CP6	-2.5 cm (-1”)
HP1	9.5 cm (3.75”)
HP2	21.6 cm (8.5”)
HP3	33.7 cm (13.25”)
HP4	45.7 cm (18”)

The optical fiber system, ODISI 6104 system was installed and a fiber was installed in Port 7 (see Table 3 for port position nomenclature). As can be seen in Figure 86, data for Test #0904201 and 0904202 has been plotted in surface plots, where the x-axis displays time, y-axis displays distance along fiber and the z-axis, or color, is temperature. The manufacturer’s listed measurement uncertainty is ±0.6 °C. The hot pool region begins at around 4m and spans to 4.6m, the cold pool region spans from 4.6-5m. As can be seen in TEST 0904201, after activating the immersion heater,

the hot pool develops a slight stratification. Referencing Table 7 we see that the bottom IHX outlet (#1) is utilized resulting in a quite isothermal temperature profile after the hot water is injected into the cold pool at around 300 seconds. Conversely, looking at TEST 0904202, where the top IHX outlet (#6) is used, there is significant thermal stratification in the cold pool (4.6-5 m) starting at around 300 seconds. This leads to an injection of hot water into the hot pool at around 600 seconds as the intake for the pump is located at the very top of the cold pool. This behavior is repeated in TEST 0904203 and 0904204, with increased thermal stratification in 0904203 when the top most IHX outlet is used.

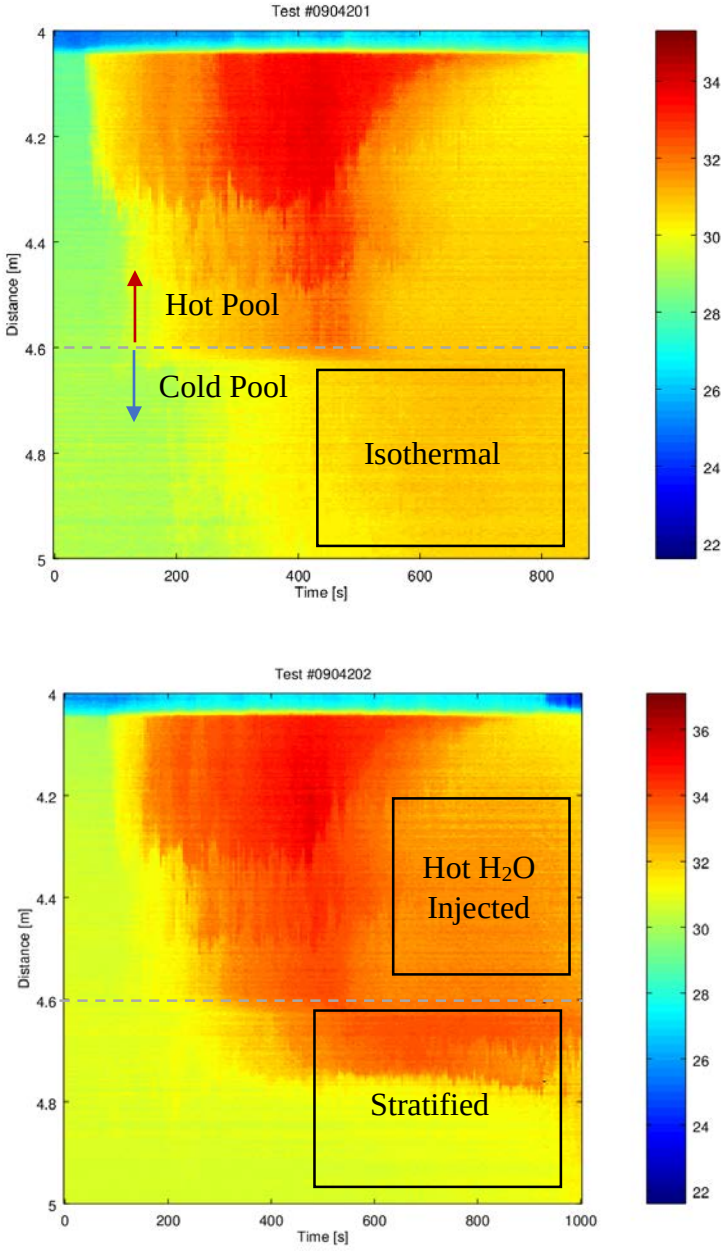

Figure 86: Optical fiber data for Test # 0904201 (top) and 0904202 (btm). Hot pool region spans from 4-4.6 [m], cold pool region spans from 4.6-5 [m]. The color bar displays temperature in degrees C.

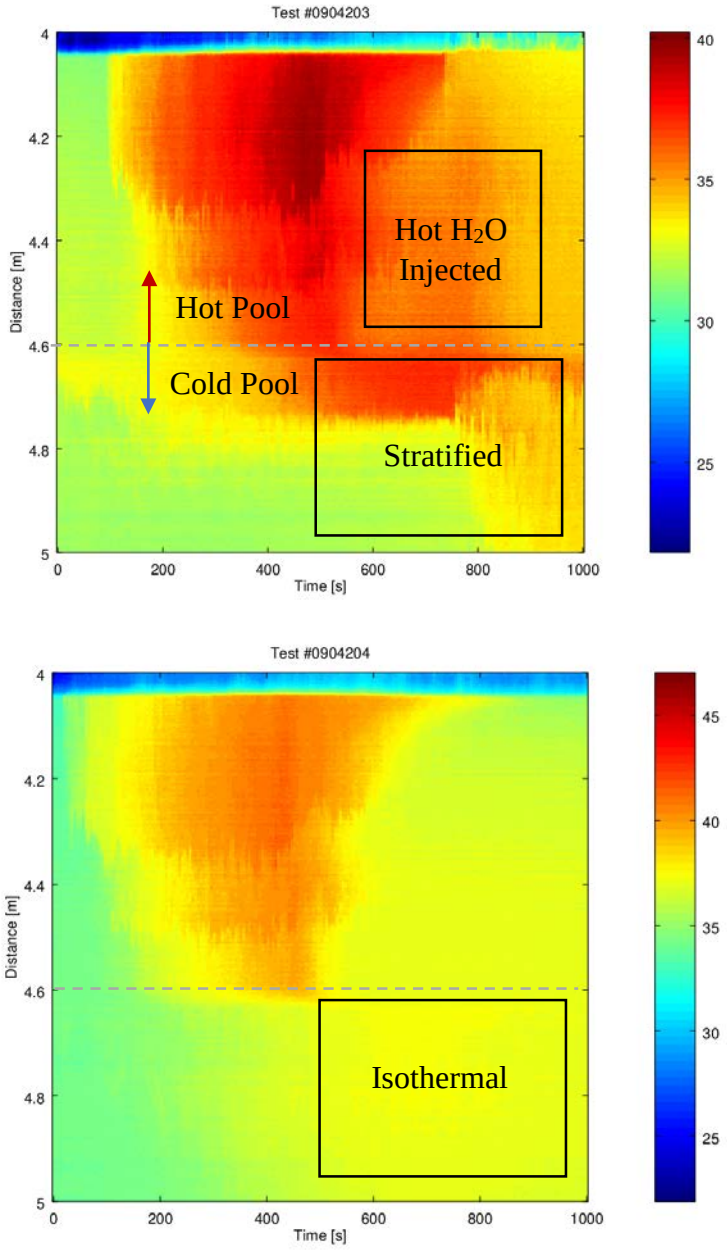

Figure 87: Optical fiber data for Test # 0904203 (top) and 0904204 (btm). Hot pool region spans from 4-4.6 [m], cold pool region spans from 4.6-5 [m]. The color bar displays temperature in degrees C.

6. THETA Model Development

Modeling of the Thermal Hydraulic Experimental Test Article (THETA) experiment has been performed using the SAS4A/SASSYS-1 fast reactor safety analysis code. A THETA model has been developed to represent the THETA experiment design developed at Argonne to demonstrate the importance of key elevations on natural circulation flow rates. The model currently includes the core channel and the primary heat transport system of the THETA experimental facility. A summary of this work can be found in [1].

7. Conclusions and Path Forward

All major components for the primary system have been acquired and dry assembled. Commissioning and testing of the major primary system components is nearing completion using deionized water. Design work on the secondary system is nearing completion, the air-to-sodium heat exchanger is on site and ready for installation, this represents the longest lead time component so this will prevent delay when beginning secondary loop construction. Given the rigor of design work and safety analysis on the facility and the collaboration of designers with systems code developers, THETA will be an important asset for the METL facility and for sodium cooled reactor component and code development.

8. Acknowledgements

The authors would like to acknowledge the rest of the Mechanisms Engineering Test Loop (METL) team, Anthony Reavis and Daniel Andujar, for all of their hard work and dedication to constructing, maintaining and operating the facility. The authors would also like to acknowledge Dzmitry Harbaruk and Henry Belch for their assistance in monitoring METL systems during 24-hour operations. This work is funded by the U.S. Department of Energy Office of Nuclear Energy's Advanced Reactor Technologies program. A special acknowledgement goes to Mr. Brian Robinson, Fast Reactor Program Manager for the DOE-NE ART program and to Dr. Robert Hill, the National Technical Director for Fast Reactors for the DOE-NE ART program for their consistent support of the Mechanisms Engineering Test Facility and its associated experiments, including the Thermal Hydraulic Experimental Test Article (THETA). Prior years' support has also been provided by Mr. Thomas O'Connor, Ms. Alice Caponiti, and Mr. Thomas Sowinski of U.S. DOE's Office of Nuclear Energy.

9. References

[1] M. Weathered *et al.*, "Thermal Hydraulic Experimental Test Article – Status Report for FY2019 Rev. 1," Lemont, 2019.

[2] T. Sumner and A. Moisseytsev, "Simulations of the EBR-II Tests SHRT-17 and SHRT-45R," in *16th International Topical Meeting on Nuclear Reactor Thermal Hydraulics (NURETH-16)*, 2015.

[3] W. Logie, C. Asselineau, J. Pye, and J. Coventry, "Temperature and Heat Flux Distributions in Sodium Receiver Tubes," no. December, 2015.

[4] E. Skupinski, J. Tortel, and L. Vautrey, "Determination des coefficients de convection d'un alliage sodium-potassium dans un tube circulaire," *Int. J. Heat Mass Transf.*, vol. 8, no. 6, pp. 937–951, 1965.

[5] Maresca and Dwyer, "Heat Transfer to Mercury Flowing In-Line Through a Bundle of Circular Rods," *Trans. ASME*, 1964.

[6] Foust, *Sodium-NaK Engineering Handbook Vol II*. 1979.

[7] W. C. Gray and E. R. Astley, "Liquid Metal Magnetic Flowmeters," *J. Instrum. Soc. Am.*, 1954.

[8] K. Terrani, R. Dehoff, R. Duncan, and F. List, "Email Correspondence on 3D Printed Impeller with ORNL." 2020.

[9] N. Tanaka, S. Moriya, S. Ushijima, and T. Koga, "Prediction method for thermal stratification in a reactor vessel," *Nucl. Eng. Des.*, vol. 120, pp. 395–402, 1990.

Nuclear Science and Engineering
Argonne National Laboratory
9700 South Cass Avenue, Bldg. 208
Argonne, IL 60439

www.anl.gov

Argonne National Laboratory is a U.S. Department of Energy laboratory managed by UChicago Argonne, LLC